Centrophilic retrotransposon integration via CENH3 chromatin in *Arabidopsis*

https://doi.org/10.1038/s41586-024-08319-7

Received: 18 April 2024

Accepted: 31 October 2024

Published online: 1 January 2025

Open access

Check for updates

Sayuri Tsukahara[1]✉, Alexandros Bousios[2]✉, Estela Perez-Roman[2], Sota Yamaguchi[1], Basile Leduque[3], Aimi Nakano[1], Matthew Naish[4], Akihisa Osakabe[1], Atsushi Toyoda[5], Hidetaka Ito[6], Alejandro Edera[3], Sayaka Tominaga[1], Juliarni[1], Kae Kato[7], Shoko Oda[1], Soichi Inagaki[1], Zdravko Lorković[8], Kiyotaka Nagaki[9], Frédéric Berger[8], Akira Kawabe[10], Leandro Quadrana[3], Ian Henderson[4] & Tetsuji Kakutani[1]✉

In organisms ranging from vertebrates to plants, major components of centromeres are rapidly evolving repeat sequences, such as tandem repeats (TRs) and transposable elements (TEs), which harbour centromere-specific histone H3 (CENH3)[1,2]. Complete centromere structures recently determined in human and *Arabidopsis* suggest frequent integration and purging of retrotransposons within the TR regions of centromeres[3–5]. Despite the high impact of 'centrophilic' retrotransposons on the paradox of rapid centromere evolution, the mechanisms involved in centromere targeting remain poorly understood in any organism. Here we show that both *Ty3* and *Ty1* long terminal repeat retrotransposons rapidly turnover within the centromeric TRs of *Arabidopsis* species. We demonstrate that the *Ty1/Copia* element *Tal1* (*Transposon of Arabidopsis lyrata 1*) integrates de novo into regions occupied by CENH3 in *Arabidopsis thaliana*, and that ectopic expansion of the CENH3 region results in spread of *Tal1* integration regions. The integration spectra of chimeric TEs reveal the key structural variations responsible for contrasting chromatin-targeting specificities to centromeres versus gene-rich regions, which have recurrently converted during the evolution of these TEs. Our findings show the impact of centromeric chromatin on TE-mediated rapid centromere evolution, with relevance across eukaryotic genomes.

Despite the essential and conserved functions of centromeres for chromosome transmission, they are structurally diverse and evolve rapidly, which is termed the 'centromere paradox'[1–7]. Rapid centromere evolution is associated with extremely frequent turnover of tandem repeats (TRs) and transposable elements (TEs)[3–5,7,8]. Single monomers of the centromeric TRs are typically between 100 and 200 base pairs (bp) in length, which are capable of loading one nucleosome with the centromere-specific histone H3 (CENH3) (also known as CENP-A (centromere protein A))[9–11]. A notable feature of centromeric TEs is that they contain heterochromatic marks, such as cytosine methylation (mC) and methylation of histone H3 lysine 9 (H3K9me)[11], which generate regions of reduced accessibility and repressed transcription. The centromeric TEs and associated constitutive heterochromatin significantly affect centromere functions and chromosome behaviours[9–13].

Centromeric TEs have been extensively studied at the level of sequence variation and evolution[5,14–18]. However, understanding of centromeric TE dynamics is still limited at the mechanistic level, mainly because mobile copies have not been isolated for most centromeric TEs. Here we characterize the behaviour and evolution of mobile centromeric TEs, which has revealed the impact of CENH3 chromatin on guiding integration, with implications for the dynamics and evolution of TEs and centromeres.

LTR elements in *A. lyrata* centromeres

Whereas the model plant *A. thaliana* is predominantly an inbreeding species, its sister species *Arabidopsis lyrata* is an outcrosser, the genome of which is predicted to harbour a larger number of active TEs[5,19–22]. Consistently, assembly of complete centromere structures of two natural accessions of *A. lyrata* revealed that their centromeric TR regions contain a higher proportion of integrations of the *Ty3* class of long terminal repeat (LTR) elements called *ATHILA* compared to those in *A. thaliana*[5] (Fig. 1a). The *ATHILA* copies in *A. lyrata* genome tend to be younger than those of *A. thaliana* (Fig. 1b), consistent with the idea that outcrossing *A. lyrata* genome contains more active TEs. In addition to *ATHILA*, we found that *A. lyrata* centromeric TR regions contain hundreds of insertions of *Ty1/Copia* class LTR elements called *ALE*[23,24] (Fig. 1 and Extended Data Fig. 1a). As is the case for *ATHILA*[3,5], *ALE* is abundant in the TR regions (Fig. 1d and Extended Data Fig. 1a). The centromeric TR regions contain a greater density of *ATHILA* and

[1]Department of Biological Sciences, The University of Tokyo, Tokyo, Japan. [2]School of Life Sciences, University of Sussex, Brighton, UK. [3]Institute of Plant Sciences Paris-Saclay (IPS2), Centre National de la Recherche Scientifique, Institut National de Recherche pour l'Agriculture, l'Alimentation et l'Environnement, Université Evry, Université Paris-Saclay, Gif sur Yvette, France. [4]Department of Plant Sciences, University of Cambridge, Cambridge, UK. [5]Center for Genetic Resource Information, National Institute of Genetics, Mishima, Japan. [6]Faculty of Science, Hokkaido University, Sapporo, Japan. [7]Department of Integrated Genetics, National Institute of Genetics, Mishima, Japan. [8]Gregor Mendel Institute (GMI), Austrian Academy of Sciences, Vienna BioCenter (VBC), Vienna, Austria. [9]Institute of Plant Science and Resources, Okayama University, Kurashiki, Japan. [10]Faculty of Life Sciences, Kyoto Sangyo University, Kyoto, Japan. ✉e-mail: stsukaha@g.ecc.u-tokyo.ac.jp; ab35@sussex.ac.uk; tkak@bs.s.u-tokyo.ac.jp

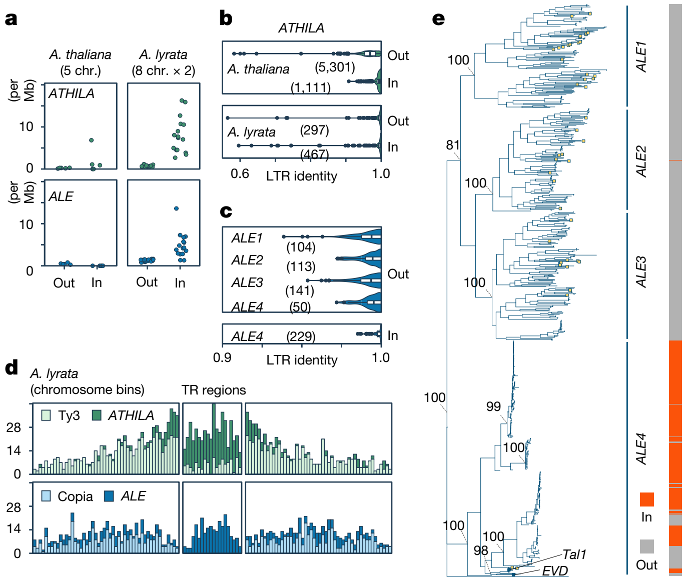

Fig. 1 | LTR elements in *A. lyrata* centromeres. a, *ATHILA* and *ALE* density shown as the number of intact insertions per Mb inside (In) and outside (Out) the TRs associated with centromeres. Each circle represents one chromosome (chr.) from the *A. thaliana* (Columbia strain) or *A. lyrata* (two strains) genome including the centromeres[3,5]. **b**, Distribution of LTR sequence identities of *ATHILA* elements in *A. lyrata* and *A. thaliana*. In and Out copies are separately characterized. Data for 66 *A. thaliana* accessions[5] are used (Methods). **c**, Distribution of LTR sequence identities of the *ALE* branches. In **b** and **c**, centre lines represent median values, box borders correspond to the first and third quartiles (interquartile range), whiskers are extended up to the largest value no further than 1.5× interquartile range, outliers are shown as black dots and the numbers of elements are shown within the parenthesis. **d**, The number of intact *Ty1/Copia*, *ALE*, *Ty3* and *ATHILA* insertions in the TR and surrounding areas. The TRs were split into 20 bins of varying size, depending on their length. The mean size of these bins was used for 50 upstream and downstream bins to count insertions. **e**, Phylogeny of intact *ALE* elements based on the concatenated integrase (PF00665) and reverse transcriptase (PF07727) core domains in *A. lyrata* and *A. thaliana* (yellow boxes), rooted with the *Ty1* element (M18706.1) from *Saccharomyces cerevisiae* (bottom). The four main branches are indicated, and the relationship of each element (In/Out) to the TRs (the numbers are shown in Supplementary Table 1). Bootstrap support of key nodes and the position of *Tal1* and *EVD* are shown. In this figure, *A. lyrata* genomes of NT1 from Siberia and MN47 from North America were used. A Circos plot in Extended Data Fig. 1a shows TE distribution along *A. lyrata* MN47 chromosomes.

ALE in *A. lyrata* than in *A. thaliana*, with the contrast being most evident for *ALE*, which is completely absent from the TR regions of *A. thaliana* (Fig. 1a). Centrophilic *ALE*s are prevalent in other related genera (Supplementary Discussion 1 and Extended Data Fig. 2), suggesting that they are ancestral or recurrently evolving.

Phylogenetic analysis separated *ALE* elements within *A. lyrata* genomes into four main branches (Fig. 1e). These four *ALE* clusters differ in regard to localization within the centromere-associated TR regions (Fig. 1e and Extended Data Fig. 1a), and we termed the most centrophilic branch *ALE4*. Most *ALE4* elements (229 of 279) are located within the TR regions, whereas *ALE1*, *ALE2* and *ALE3* are localized almost exclusively outside the TR regions (Fig. 1e, right, and Extended Data Fig. 1a). Compared to the *ALE1*–*ALE3* elements, *ALE4* elements within the TR regions have higher within-element LTR identity (Fig. 1c), and shorter terminal branches on the phylogenetic tree (Fig. 1e), suggesting recent integration. The lack of older *ALE4* insertions within the TR region suggests efficient removal of the elements, as has been proposed for centromeric *ATHILA* elements[5], or recent expansion of the *ALE4* clade. Taken together, we observe parallels in the dynamics of *ALE4* and *ATHILA*, two deeply divergent LTR retrotransposon lineages, both of which are suggested to frequently integrate into the TR regions and purged from there efficiently.

Neo-insertion of *Tal1* into centromeres

One of the centromeric *ALE4* copies in *A. lyrata* is *Tal1*, which is closely related to *A. thaliana COPIA93/EVADE* (*EVD*) (Fig. 1e), sharing 81.3% (1,172 of 1,442) identity along their coding amino acid sequences[25–27]. *EVD* has been shown to preferentially integrate into gene-rich regions of *A. thaliana* genome[26–28]. We have previously induced de novo *Tal1* integrations within the *A. thaliana* genome, and observed that the integrations are enriched in regions flanking the 178 bp TR sequences (CEN178)[27]. However, it remains unknown which genomic features dictate the specific integration.

Using the recently determined Col-CEN reference genome (https://github.com/schatzlab/Col-CEN), which includes complete centromere sequences[3], we profiled de novo integrations of *Tal1*. We adapted the technique of Transposable Element Display[29] for high-throughput sequencing (TEd-seq), enabling the detection of somatic neo-insertions of *Tal1* in the order of 10,000–100,000 events per sample. In all five chromosomes, *Tal1* integrations were confined to the centromeric TR regions (Fig. 2a,b and Extended Data Fig. 3a). Notably, the regions of *Tal1* integrations were strongly associated with CENH3 enrichment (Fig. 2a,b and Extended Data Fig. 3a). In *A. thaliana*, CENH3 is confined to the TR regions, but it does not evenly occupy the entire repeat array[3] (Fig. 2a). That is most clearly seen in the centromere TR arrays of chromosome 4 (*CEN4*). In *CEN4*, CENH3 mainly occupies the left half (short-arm side) of the TR clusters, and we observe that *Tal1* preferentially integrates into the CENH3-occupied array (Fig. 2a). In all five centromeres, the CENH3 signal shows a gradient of intensity within the TR regions, and the frequency of *Tal1* integration is significantly correlated with the CENH3 signal ($r = 0.67$) (Fig. 2a,c). These results are consistent with *Tal1* integration being targeted to chromatin enriched in CENH3.

As *Tal1* is structurally similar to *ATCOPIA93/EVD* (ref. 25), we also examined somatic neo-insertions of *EVD* using the TEd-seq method. We observed that *EVD* preferentially integrated into the gene-rich chromosome arm regions, but not into the pericentromeric or centromeric regions (Fig. 2b,e and Extended Data Fig. 3a), where heterochromatin marks, such as H3K9me, are enriched in wild type. We examined *EVD* transpositions in the *ddm1* (*decrease in DNA methylation*) mutant background, where heterochromatin marks, such as H3K9me and mC are lost from centromeric and pericentromeric regions[30–36]. In the *ddm1* mutant background, the genomic regions of *EVD* integration were expanded to include the pericentromeric regions, compared to those in wild type (Fig. 2b,e–g and Extended Data Fig. 3a). However, even in *ddm1*, *EVD* retrotransposition into the centromeric core TRs was not detected (Fig. 2b,e–g and Extended Data Fig. 3a,b). These features of *EVD* integration are consistent with a previous report[28], and stand in contrast to *Tal1*, which integrates into the core of centromere (Fig. 2 and Extended Data Fig. 3).

We next investigated *Tal1* integration in a *ddm1* mutant background to test the role of heterochromatic marks. The TR regions covered by CENH3 have relatively low heterochromatic marks, such as H3K9me and methyl-C in non-CpG contexts (mCH, where H = A, T or C), compared to the flanking pericentromeric heterochromatin[3]. In *ddm1*, despite the loss of heterochromatic marks in centromeric and pericentromeric regions, the distribution of *Tal1* integration measured by TEd-seq was overall similar to that in the wild-type background (Fig. 2b–d,g and Extended Data Fig. 3). We also performed whole-genome sequencing using PacBio long-read technology to map de novo *Tal1* integrations and found similar integration spectra (Fig. 2b and Extended Data Fig. 3a). Together, these results are consistent with *Tal1* possessing a key centrophilic adaptation, in contrast to the closely related *EVD* element.

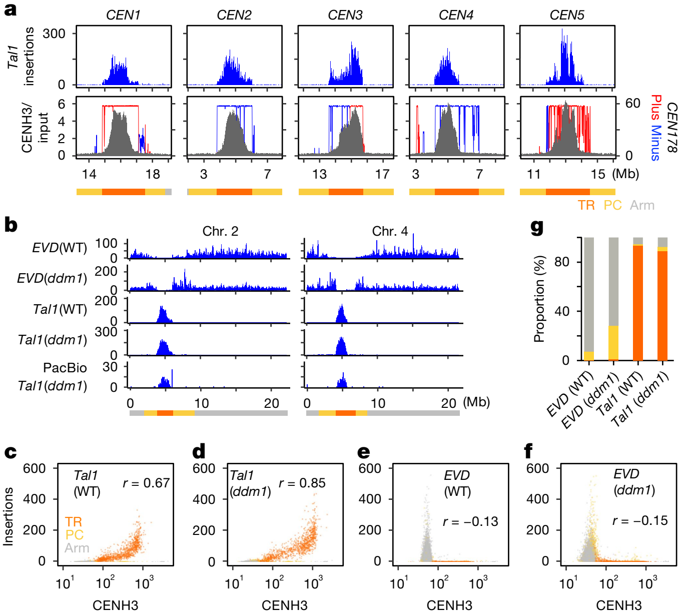

Fig. 2 | De novo *Tal1* integrations are confined to the TR regions occupied by CENH3. a, Top, distribution of somatic neo-insertions of *Tal* after introduction of a *Tal1* transgene into *A. thaliana*. Bottom, CENH3 (ChIP/input) (grey) and *CEN178* per 10 kb for forward (red) or reverse (blue) strand orientations[3]. Each of these values were counted in adjacent 10 kb intervals. TR (orange), pericentromeric (PC, yellow) and chromosomal arm (Arm, grey) regions are indicated by different colours at the bottom. **b**, Somatic neo-insertions of *EVD* and *Tal1* in wild-type and *ddm1* backgrounds. The integrations were counted in 10 kb intervals and shown by sliding windows of size 9 and step 1. *Tal1* (wild type), *Tal1* (*ddm1*) and *EVD* (wild type) show neo-insertions of respective TEs in the transgenic *A. thaliana* lines, whereas *EVD* (*ddm1*) show neo-insertions of endogenous *EVD* in the *ddm1* mutant plants without the transgene[27]. Results of chromosomes two and four are shown, and the results of all five chromosomes are shown in Extended Data Fig. 3a. Detection of *Tal1* integration by PacBio-seq are also shown in the bottom. **c**–**f**, Scatter plots comparing CENH3 enrichment and *Tal1* (**c**,**d**) or *EVD* (**e**,**f**) integration frequencies in wild-type (WT) (**c**,**e**) or *ddm1* (**d**,**f**) backgrounds. Each dot represents values in a single 10 kb interval. The Pearson correlation coefficient (*r*) is shown in each panel. **g**, Summary of integration specificities of *EVD* and *Tal1* into TR, pericentromeric and arm regions in wild-type and *ddm1* backgrounds. Proportion of integrations in each of these regions are shown. Results of extra lines are shown in Extended Data Fig. 3b.

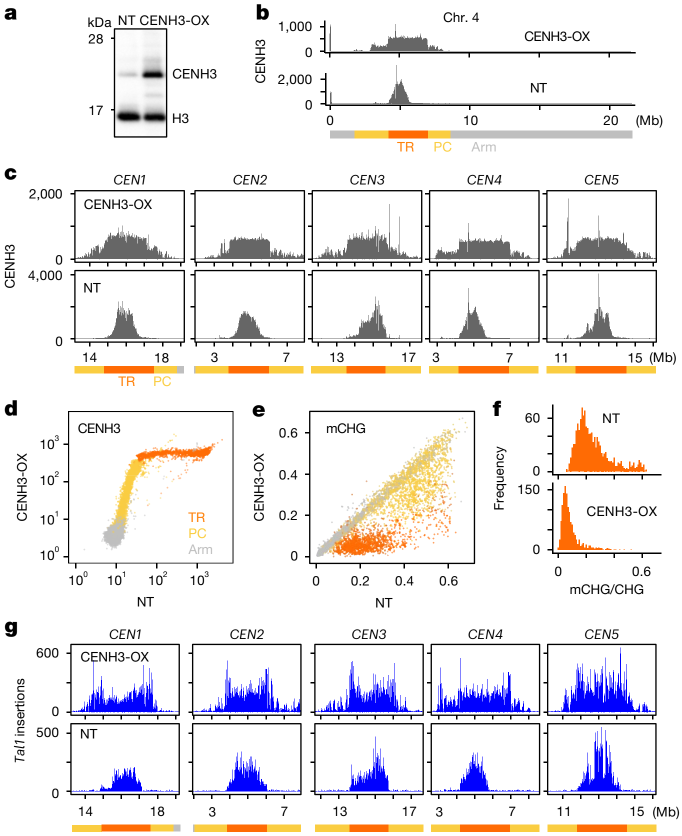

Fig. 3 | Spread of CENH3 deposition induces mirrored expansion of *Tal1* integration. a, Western blot analyses of purified nuclei from non-transgenic (NT) line and transgenic line overexpressing CENH3 (CENH3-OX). Antibody against CENH3, which is weakly cross-reactive with H3 (anti-CENH3 C-terminal antibody) is used (validation shown in Supplementary Fig. 1a,b). Biological replicates of the same conditions and with extra anti-H4 antibody and extra independent transgenic lines are shown in Extended Data Fig. 4a and Supplementary Figs. 3 and 4 (*n* = 6 in total). **b**,**c**, Overexpression of CENH3 induces expansion of genomic regions covered by CENH3. **b**, Entire chromosome. **c**, Centromeric regions. Antibody recognizing CENH3 but not H3 (anti-HTR12 (CENH3 N-terminal) antibody) is used (validation in Supplementary Fig. 1a,b). ChIP–seq profiles of CENH3 (normalized by million total mapped reads and counted in 10 kb intervals) are shown for NT and CENH3-OX line. CENH3 profiles in other independent transgenic lines are shown in Extended Data Fig. 4b,c. **d**, Genome-wide comparison of CENH3 levels between wild type and the CENH3-OX backgrounds. Each dot represents a single 10 kb region, with different colours for TR, pericentromere and arm regions. **e**, DNA mCHG level of the CENH-OX line compared to parental NT line. **f**, Histogram of mCHG level in centromeric TR regions shown for 10 kb units. **g**, Distribution of *Tal1* integrations compared between sibling plants with and without the CENH3-OX transgene, both in the *ddm1* mutant background. Results of F_2 plants in *DDM1* wild-type and the *ddm1* mutant backgrounds for two independent CENH3-OX families and F_1 plants are shown in Extended Data Fig. 5.

CENH3 defines region of *Tal1* integration

As regions of *Tal1* integration match closely to the regions occupied by CENH3, we examined the effects of change in CENH3 distribution on retrotransposition. To modify CENH3 distribution, we overexpressed this protein in the wild-type Col-0 background under the constitutively active promoter *RPS5a* (ref. 37). In the lines with CENH3 overexpression (hereafter referred to as CENH3-OX), the amount of chromatin-bound CENH3 increased (Fig. 3a and Extended Data Fig. 4a), and the CENH3-occupied parts of TRs significantly expanded in all five chromosomes (Fig. 3b,c and Extended Data Fig. 4b). Although CENH3 covers only part of the TR regions in non-transgenic (NT) Col-0 plants, CENH3 covers the entire TR regions in the CENH3-OX lines (Fig. 3b–d and Extended Data Fig. 4b,c). In addition, whereas wild-type CENH3 distribution shows a gradient of enrichment, with a peak towards the centre of the TR arrays, the arrays appear fully CENH3 occupied in CENH3-OX, consistent with saturated deposition (Fig. 3c,d and Extended Data Fig. 4b,c). In CENH3-OX, mCHG levels in the TR regions and pericentromeric regions decreased (Fig. 3e,f), probably because CENH3 does not have H3K9, and H3K9me is required to maintain DNA mCHG (refs. 38–40). Levels of mCHG in the TR regions were decreased in CENH3-OX to the level one order of magnitude lower than the maximum level seen in the non-transgenic controls, further supporting the interpretation that TR regions become saturated with CENH3-loaded nucleosomes in the CENH3-OX lines (Fig. 3e,f).

We next examined the effects of CENH3 overexpression on the integration of *Tal1*, using progeny from crosses between the transgenic lines expressing *Tal1* and CENH3-OX. In the CENH3-OX background, *Tal1* integration was found across the entire TR regions (Fig. 3g and Extended Data Fig. 5). Expanded *Tal1* integration was clearly observed in *CEN4*, where the spread of *Tal1* integration into the right half of the TR cluster parallels the spread of CENH3 signal to the entire TR regions in CENH3-OX (Fig. 3g and Extended Data Fig. 5). In both *ddm1* and wild-type backgrounds of CENH3-OX lines, *Tal1* integration spreads into the entire TR regions, which mirrors the change in CENH3 distribution. A subset of the CENH3-OX lines also shows *Tal1* integration outside the TR regions (Fig. 3g and Extended Data Fig. 5), which parallels the expansion of CENH3 into pericentromeric regions (Fig. 3b–d and Extended Data Fig. 4b,c). Together, these results directly demonstrate that *Tal1* is targeted to CENH3 chromatin in vivo (further discussion in Supplementary Discussion 2).

Genetic basis for the integration bias

Tal1 is targeted to CENH3 chromatin, whereas *EVD* is targeted to the gene-rich chromosome arm regions (Fig. 2). To explore the genetic basis within the *Tal1* and *EVD* sequences for their different integration preferences, we generated chimeric constructs and examined their integration spectra genome wide (Fig. 4). We tested regions containing the conserved domain of integrase (IN1), in addition to the more diverse C-terminal region (IN2) (Supplementary Fig. 2a), as examples are known that integrases define target site specificities[41–44]. Chimeric constructs carrying IN2 from *Tal1* within a *EVD* backbone (*EVD*_IN2_T) were found to specifically integrate into the centromere TR arrays (Fig. 4a and Extended Data Fig. 6). Conversely, chimeric constructs with IN2 region from *EVD* in a *Tal1* backbone (*Tal1*_IN2_E) integrated into the chromosome arm regions (Fig. 4a and Extended Data Fig. 6). Analogous chimeric constructs of IN1 regions did not induce changes in element integration specificities (Fig. 4a and Extended Data Fig. 6). These results demonstrate that the C-terminal region of integrase is responsible for the strong integration preferences of *Tal1* and *EVD* into the centromeres versus the chromosome arms, respectively.

We further inspected the IN2 regions of *Tal1* and *EVD* to identify causal polymorphisms that may dictate integration preference. Among the structural variations within the IN2 region examined (Supplementary Fig. 2b), an R/K non-synonymous polymorphism has a strong effect on the target site specificity (Fig. 4b,c and Extended Data Fig. 7). R892K substitution in the coding region of *Tal1* converts its integration specificity to that of *EVD* (*Tal1* (R892K) in Fig. 4b,c and Extended Data Fig. 7). Compared to the replacement of the entire IN2 region (*Tal1*_IN2_E in Fig. 4a), however, low but significant integrations into the centromeric TR regions were still detected in *Tal1* (R892K), suggesting that extra variation within the IN2 region may contribute to target site preference. Conversely, the K854R substitution of *EVD* significantly changes integration specificity from that seen with either *EVD* or *Tal1* (Fig. 4b,c and Extended Data Fig. 7). Specifically, highest *EVD* (K854R) integration rates were observed in the pericentromeric regions, with low levels of integration into the centromeric TRs. Thus, single R/K substitution within the C-terminal of integrase has a strong impact on retrotransposon integration specificities, and governs the contrasting centrophilic versus centrophobic integration specificities of *Tal1* and *EVD*. The switches between the contrasting target specificities are also suggested by the phylogenetic analysis shown below.

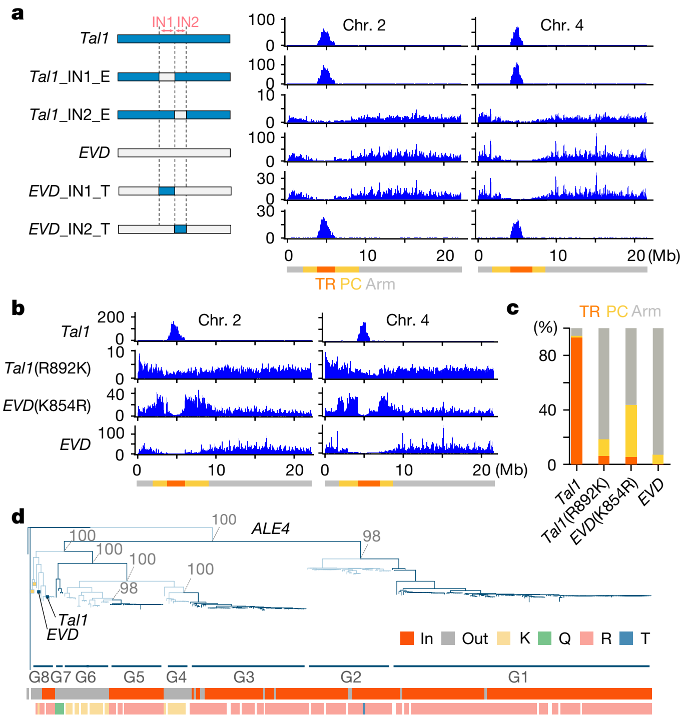

Fig. 4 | Mapping of integrase regions that define the centrophilic versus centrophobic integrations. a, De novo somatic insertions of each chimeric TE examined by TEd-seq. Structure of each chimeric TE is shown schematically in the left. IN1 and IN2 correspond to conserved domains of integrase and its C-terminal regions, respectively (Supplementary Fig. 2). Blue and grey indicate the sequence of *Tal1* and *EVD*, respectively. Integration spectra of chromosomes 2 and 4 are shown; the results of all five chromosomes, and also further transgenic lines are shown in Extended Data Fig. 6a,b. **b**, R/K substitutions in *Tal1* or *EVD* integrase IN2 region changes integration specificities. Positions of the substitutions are shown in Extended Data Fig. 5b. Results of chromosomes 2 and 4 for one transgenic line for each genotype are shown. Results in the all five chromosomes and also chromosome 4 of multiple independent transgenic lines are shown in Extended Data Fig. 7. **c**, Summary of proportions of integration frequency of *EVD*, *Tal1* and their K/R substitution constructs into TR, pericentromere and arm regions. **d**, The phylogeny within the *ALE4* clade. Groups G1–8 are shown in alternating dark and light blue shading. The bottom strips show the relationship to the TR position (in/out), and the amino acid polymorphisms R, K and others. Blank positions reflect copies difficult to align. Sequence similarity levels between G1–8 are shown in Extended Data Fig. 8c, whereas their copy numbers with the in/out locations are shown in Supplementary Table 2.

Evolution of the integration bias

Analogous K/R substitutions are also observed among *ALE4* copies other than *Tal1* and *EVD*. On the basis of phylogenetic relationships and the levels of sequence similarity, we subdivided *ALE4* into eight groups, G1–G8 (Fig. 4d and Extended Data Fig. 8). The centrophilic *Tal1* and centrophobic *EVD* both belong to G8. Among the other groups, G3–G6 members share high level of similarities in the overall sequence (Fig. 4d and Extended Data Fig. 8c); however, G4 and G6 are exclusively centrophobic, whereas G3 and G5 are nearly always localized inside the *A. lyrata* centromeric TR regions (Fig. 4d). The centrophobic G4 and G6 members have longer terminal branches on the phylogenetic tree compared to centrophilic G3 or G5 (Fig. 4d). Notably, the centrophobic distribution of G4 and G6 and centrophilic distribution of G3 and G5 (and also G1 and G2) are strongly associated with the R/K substitution (Fig. 4d bottom and Extended Data Fig. 8d), which govern the contrasting integration specificities of *Tal1* and *EVD* within G8. Thus, the drastic changes in the integration spectra induced by K/R substitutions in *Tal1* and *EVD* (Fig. 4b,c), are reflected by recurrent evolutionary conversions of this site, which is associated with centrophilic versus centrophobic properties (there is further discussion about their conserved mode of integration in Supplementary Discussion 3 and Extended Data Figs. 9 and 10).

Discussion

We characterized control of the de novo targeting of the centrophilic LTR retrotransposon *Tal1*. Although centromeric retroelements are commonly observed across eukaryotes, the mechanistic characterization of their integration preference remains incomplete in any organism. Notably, however, it was recently shown that a K to R amino acid substitution in the HIV-1 integrase C-terminal domain causes this retrovirus to integrate into the centromeres, instead of genic regions[45,46]. Our results showed that analogous reversible and recurrent K/R substitutions within *ALE4* integrase C-terminal domains control evolution of centrophilic versus centrophobic integration preferences (there is further discussion about the C-terminal domain of integrases in Supplementary Discussion 4). In addition, expansion of the TR regions occupied by CENH3 results in a mirrored expansion of *Tal1* integration, consistent with centromeric chromatin dictating *Tal1* integration. Mechanistically, it will be interesting to investigate how the centrophilic properties of *Tal1* are related to convergent adaptations in *ATHILA* and other centrophilic TEs[3,5].

Despite the large variation in the size of centromeric TRs in natural accessions of *A. thaliana*, the regions covered by CENH3 remains nearly constant, suggesting underlying homeostatic mechanisms[5]. This homeostasis seems to depend on CENH3 expression level, as the CENH3-OX lines show the spreading of regions occupied by CENH3. Although CENH3 localization shows a gradient of accumulation in wild-type centromeres, CENH3-OX lines instead show a plateau of CENH3 accumulation, which parallels loss of heterochromatic marks. The CENH3-OX lines are viable and fertile, as is the case for a variety of *Arabidopsis* mutants of the chromatin components and modifiers[11,13,40,47–49]. Further genetic studies of the interplay among chromatin proteins, TRs and centrophilic TEs will provide mechanistic understanding of chromosome and centromere evolution conserved across eukaryotes.

Online content

Any methods, additional references, Nature Portfolio reporting summaries, source data, extended data, supplementary information, acknowledgements, peer review information; details of author contributions and competing interests; and statements of data and code availability are available at https://doi.org/10.1038/s41586-024-08319-7.

1. Henikoff, S., Ahmad, K. & Malik, H. S. The centromere paradox: stable inheritance with rapidly evolving DNA. *Science* **293**, 1098–1102 (2001).
2. Malik, H. S. & Henikoff, S. Major evolutionary transitions in centromere complexity. *Cell* **138**, 1067–1082 (2009).
3. Naish, M. et al. The genetic and epigenetic landscape of the *Arabidopsis* centromeres. *Science* **374**, eabi7489 (2021).
4. Altemose, N. et al. Complete genomic and epigenetic maps of human centromeres. *Science* **376**, eabl4178 (2022).
5. Wlodzimierz, P. et al. Cycles of satellite and transposon evolution in *Arabidopsis* centromeres. *Nature* **618**, 557–565 (2023).
6. Ekwall, K. Epigenetic control of centromere behavior. *Annu. Rev. Genet.* **41**, 63–81 (2007).
7. Yan, A. & Yu, H. New insights into centromeres from *Arabidopsis* Col-CEN assembly. *Trends Genet.* **38**, 416–418 (2022).
8. Courret, C. et al. Rapid turnover of centromeric DNA reveals signatures of genetic conflict in *Drosophila*. Preprint at *bioRxiv* https://doi.org/10.1101/2023.08.22.554357 (2023).
9. Ohzeki, J., Larionov, V., Earnshaw, W. C. & Masumoto, H. De novo formation and epigenetic maintenance of centromere chromatin. *Curr. Opin. Cell Biol.* **58**, 15–25 (2019).
10. Talbert, P. & Henikoff, S. Centromere drive: chromatin conflict in meiosis. *Curr. Opin. Genet. Dev.* **77**, 102005 (2022).
11. Fukagawa, T. & Kakutani, T. Transgenerational epigenetic control of constitutive heterochromatin, transposons, and centromeres. *Curr. Opin. Genet. Dev.* **78**, 102021 (2023).
12. Dudka, D. & Lampson, M. A. Centromere drive: model systems and experimental progress. *Chromosome Res.* **30**, 187–203 (2022).
13. Shimada, A. et al. Retrotransposon addiction promotes centromere function via epigenetically activated small RNAs. *Nat. Plants* **10**, 1304–1316 (2024).
14. Nagaki, K. et al. Structure, divergence, and distribution of the CRR centromeric retrotransposon family in rice. *Mol. Biol. Evol.* **22**, 845–855 (2005).
15. Wolfgruber, T. K. et al. Maize centromere structure and evolution: sequence analysis of centromeres 2 and 5 reveals dynamic Loci shaped primarily by retrotransposons. *PLoS Genet.* **5**, e1000743 (2009).
16. Wu, J. et al. Comparative analysis of complete orthologous centromeres from two subspecies of rice reveals rapid variation of centromere organization and structure. *Plant J.* **60**, 805–819 (2009).
17. Sharma, A. & Presting, G. G. Centromeric retrotransposon lineages predate the maize/rice divergence and differ in abundance and activity. *Mol. Genet. Genomics* **279**, 133–147 (2008).
18. Sharma, A. & Presting, G. G. Evolution of centromeric retrotransposons in grasses. *Genome Biol. Evol.* **6**, 1335–1352 (2014).
19. Hickey, D. A. Selfish DNA: a sexually-transmitted nuclear parasite. *Genetics* **101**, 519–531 (1982).
20. Arkhipova, I. & Meselson, M. Deleterious transposable elements and the extinction of asexuals. *Bioessays* **27**, 76–85 (2005).
21. Hu, T. T. et al. The *Arabidopsis lyrata* genome sequence and the basis of rapid genome size change. *Nat. Genet.* **43**, 476–481 (2011).
22. Burns, R. et al. Gradual evolution of allopolyploidy in *Arabidopsis suecica*. *Nat. Ecol. Evol.* **5**, 1367–1381 (2021).
23. Wicker, T. & Keller, B. Genome-wide comparative analysis of copia retrotransposons in Triticeae, rice, and *Arabidopsis* reveals conserved ancient evolutionary lineages and distinct dynamics of individual copia families. *Genome Res.* **17**, 1072–1081 (2007).
24. Neumann, P., Novák, P., Hoštáková, N. & Macas, J. Systematic survey of plant LTR-retrotransposons elucidates phylogenetic relationships of their polyprotein domains and provides a reference for element classification. *Mob. DNA* **10**, 1 (2019).
25. Tsukahara, S. et al. Bursts of retrotransposition reproduced in *Arabidopsis*. *Nature* **461**, 423–426 (2009).
26. Mirouze, M. et al. Selective epigenetic control of retrotransposition in *Arabidopsis*. *Nature* **461**, 427–430 (2009).
27. Tsukahara, S. et al. Centromere-targeted de novo integrations of an LTR retrotransposon of *Arabidopsis lyrata*. *Genes Dev.* **26**, 705–713 (2012).
28. Quadrana, L. et al. Transposition favors the generation of large effect mutations that may facilitate rapid adaption. *Nat. Commun.* **10**, 3421 (2019).
29. Casa, A. M. et al. The MITE family heartbreaker (Hbr): molecular markers in maize. *Proc. Natl Acad. Sci. USA* **97**, 10083–10089 (2000).
30. Vongs, A., Kakutani, T., Martienssen, R. A. & Richards, E. J. *Arabidopsis thaliana* DNA methylation mutants. *Science* **260**, 1926–1928 (1993).
31. Jeddeloh, J. A., Stokes, T. L. & Richards, E. J. Maintenance of genomic methylation requires a SWI2/SNF2-like protein. *Nat. Genet.* **22**, 94–97 (1999).
32. Gendrel, A.-V., Lippman, Z., Yordan, C., Colot, V. & Martienssen, R. A. Dependence of heterochromatic histone H3 methylation patterns on the *Arabidopsis* gene DDM1. *Science* **297**, 1871–1873 (2002).
33. Soppe, W. J. J. et al. DNA methylation controls histone H3 lysine 9 methylation and heterochromatin assembly in *Arabidopsis*. *EMBO J.* **21**, 6549–6559 (2002).
34. Zemach, A. et al. The *Arabidopsis* nucleosome remodeler DDM1 allows DNA methyltransferases to access H1-containing heterochromatin. *Cell* **153**, 193–205 (2013).
35. Osakabe, A. et al. The chromatin remodeler DDM1 prevents transposon mobility through deposition of histone variant H2A.W. *Nat. Cell Biol.* **23**, 391–400 (2021).
36. Lee, S. C. et al. Chromatin remodeling of histone H3 variants by DDM1 underlies epigenetic inheritance of DNA methylation. *Cell* **186**, 4100–4116.e15 (2023).
37. Maruyama, D. et al. Independent control by each female gamete prevents the attraction of multiple pollen tubes. *Dev. Cell* **25**, 317–323 (2013).
38. Jackson, J. P., Lindroth, A. M., Cao, X. & Jacobsen, S. E. Control of CpNpG DNA methylation by the KRYPTONITE histone H3 methyltransferase. *Nature* **416**, 556–560 (2002).
39. Malagnac, F., Bartee, L. & Bender, J. An *Arabidopsis* SET domain protein required for maintenance but not establishment of DNA methylation. *EMBO J.* **21**, 6842–6852 (2002).
40. To, T. K. & Kakutani, T. Crosstalk among pathways to generate DNA methylome. *Curr. Opin. Plant Biol.* **68**, 102248 (2022).
41. Bushman, F. D. Targeting survival: integration site selection by retroviruses and LTR-retrotransposons. *Cell* **115**, 135–138 (2003).
42. Gao, X., Hou, Y., Ebina, H., Levin, H. L. & Voytas, D. F. Chromodomains direct integration of retrotransposons to heterochromatin. *Genome Res.* **18**, 359–369 (2008).
43. Sultana, T., Zamborlini, A., Cristofari, G. & Lesage, P. Integration site selection by retroviruses and transposable elements in eukaryotes. *Nat. Rev. Genet.* **18**, 292–308 (2017).
44. Maertens, G. N., Engelman, A. N. & Cherepanov, P. Structure and function of retroviral integrase. *Nat. Rev. Microbiol.* **20**, 20–34 (2022).
45. Winans, S. et al. A point mutation in HIV-1 integrase redirects proviral integration into centromeric repeats. *Nat. Commun.* **13**, 1474 (2022).
46. Marquis, K. A. et al. The HIV-1 capsid-targeted inhibitor GSK878 alters selection of target sites for HIV DNA integration. *AIDS Res. Hum. Retroviruses* https://doi.org/10.1089/AID.2022.0161 (2023).
47. Wendte, J. M. & Schmitz, R. J. Specifications of targeting heterochromatin modifications in plants. *Mol. Plant* **11**, 381–387 (2018).
48. Jiang, D. & Berger, F. Variation is important: warranting chromatin function and dynamics by histone variants. *Curr. Opin. Plant Biol.* **75**, 102408 (2023).
49. Marimuthu, M. P. A. et al. Epigenetically mismatched parental centromeres trigger genome elimination in hybrids. *Sci. Adv.* **7**, eabk1151 (2021).

Publisher's note Springer Nature remains neutral with regard to jurisdictional claims in published maps and institutional affiliations.

Methods

Plant materials and growth conditions

The *A. thaliana* Columbia-0 (Col-0) accession of wild type and the *ddm1-1* mutant[30] were used throughout. The seeds were germinated on a plate of 0.5× or 1× Murashige and Skoog medium. After keeping in dark at 4 °C for 2–3 days, the plants were grown at 22 °C under long-day conditions of 16 h of light and 8 h of dark. Plant samples were harvested directly from the plate or transferred to soil for genetics.

TEd-seq library construction

A detailed protocol for TEd-seq[50] can be found at https://www.protocols.io/view/ted-seq-c7seznbe. Before preparation of the TEd-seq library, 30 µM of custom oligonucleotide adaptor was prepared as follows: 90 µl of 100 µM P7_adapter_up (5′-GTGACTGGAGTTCAGACGTGTGCTCTTCCGATC*T-3′, *phosphorothioate bond), 90 µl of 100 µM P7_adapter_bottom (5′-pGATCGGAAGAGCATC**−3′, p denotes phosphorylation, **dideoxy-C), 30 µl of T4 ligase buffer and 90 µl of H_2O were mixed. The mixture was heated at 95 °C for 2 min and cooled to 25 °C over 45 min. The TEd-seq library was prepared as follows. In most samples (see Supplementary Table 3 for details), genomic DNA was extracted from roughly 30 10-day-old seedlings using Nucleon Phytopure DNA extraction kit (GE Healthcare). Next. 500 ng of genomic DNA was suspended in 100 µl of TE buffer and sheared into the length of 250–500 bp using Bioruptor Pico (Diagenode) for three cycles of 30 s on/30 s off. The sheared DNA was cleaned up using 0.9× SPRIselect (Beckman Coulter), resuspended in 25 µl of 0.1× TE buffer and subsequently END-repaired, A-tailed and ligated to custom oligonucleotide adaptors using NEBNext Ultra II DNA Library Prep Kit for Illumina (NEB) with the reaction scale by half. Adaptor-ligated DNA was size selected using 0.13× SPRIselect for first and second bead addition, and eluted in 15 µl of 10 mM Tris-HCl pH 8.0. Then, nested PCR was performed to enrich fragments containing the terminal sequence of specific TE. For the first PCR, 7.5 µl of purified adaptor ligated DNA, 2.5 µl of adaptor specific primer, 2.5 µl of TE specific primer, 12.5 µl of NEBNext Ultra II Q5 Master Mix were mixed and PCR amplified with the following condition: 98 °C for 30 s, 20 cycles of (98 °C for 10 s, 61 °C for 75 s), 61 °C for 5 min. The primer sequences used in first PCR are shown in Supplementary Table 4. The first PCR product was cleaned up using 0.9× SPRIselect and eluted in 15 µl of 0.1× TE. The purified first PCR product was diluted ten times with 0.1× TE and used as a template in second PCR. In the second PCR, P7_primers with index and P5_TE_primers with index shown in Supplementary Table 4 were used for dual indexing. Then, 2.5 µl of first PCR product, 6.25 µl of NEBNext Ultra II Q5 Master Mix, 1.25 µl of P7_primer with index, 1.25 µl of P5_TE_primer with index, 1.25 µl of H_2O were mixed and amplified under the following conditions: 98 °C for 30 s, two cycles of 98 °C for 10 s, 61 °C for 75 s, eight cycles of 98 °C 10 s, 72 °C for 75 s, 72 °C for 5 min. The second PCR product was cleaned up with 0.9× SPRIselect and diluted in 15 µl of 0.1× TE. The final library product should contain 41 and 61 bp of the 5′ LTR terminal sequences of Tal1 and Evade, respectively. Sequencing was performed at Macrogen Japan Corp., using the Illumina Hiseq X platform or Novaseq X with a read length of 151 bp. The detailed experimental conditions for library preparation are shown in Supplementary Table 3.

TEd-seq analysis

Source code for the TEd-seq analysis can be accessed at (https://github.com/LeanQ/TED_seq_Tsukahara_2024). Briefly, TEd-seq fastq files were mapped to the 5′ terminal sequence of TE (1–144 bp of *Evade* or 1–105 bp of *Tal1* shown in the file of 'target_TE_sequence_extremity.fa') using Bowtie2 (v.2.5.3)[51] with the parameter '--local --very-sensitive'. Pair-end reads in which only one mate mapped over 5′ terminal sequence of TE were extracted using Picard tools (v.2.27.5) (https://broadinstitute.github.io/picard/) with the function of 'FilterSamReads' and then extracted discordantly mapped reads. Those reads were then mapped to Col-CEN_v1.2 reference genome using Bowtie2 with the parameter '--local --very-sensitive', and the mapped data was converted to BAM files using SAMtools (v.1.9) to generate 'clip_disc-local.sorted.bam' files. To detect de novo somatic insertions of TEs, clip_disc-local.sorted.bam files were converted to bedfiles using BEDTools (v.2.31.1)[52] with the 'bamtobed' function. The sequence reads that contain de novo insertion site should be soft-clipped reads, in which the terminal sequence of TE is soft-clipped. Within the soft-clipped reads, the start position of alignment to the reference, which is the flanking nucleotide of soft-clipped region was regarded as an insertion site. The reads mapped within the upstream 1 kilobase (kb) and downstream 1 kb of the regions that are annotated as *Evade* (AT5TE20395) and its related copy (AT1TE41580) (shown in the file of 'targeted_TE_sequences.bed') were removed using the 'intersect' function of BEDTools, as they are not de novo insertions. The reads mapped to 1–30 kb of chromosome 2 were also removed as they were systematically found in all samples, including wild-type controls, and therefore do not correspond to bona fide de novo insertions. To obtain genome-wide integration landscapes, the number of insertion sites without duplicates were counted in non-overlapping 10 kilobase pair (kbp) windows genome wide using the 'coverage' function of BEDTools. The number of insertion sites were plotted using the packages of ggplot2 (v.3.4.4)[53], readr (v.2.1.5)[54] and dplyr (v.1.1.4)[55] in R software (v.4.3.2)[56].

DNA extraction for PacBio sequencing

Genomic DNA was extracted from 2 g of aerial parts of 25-day-old *Tal1* transgenic plants (*ddm1* mutant background), which were put in dark place for 2 days before sampling. Genomic DNA was extracted by the method of Carlson lysis buffer containing cetyl trimethyl ammonium bromide (CTAB)[57] using Genomic-tip (Qiagen) in the following conditions. The frozen plant tissue was ground with a mortar and a pestle with liquid nitrogen into fine powder, and put it into Carlson lysis buffer (100 mM Tris-HCl pH 9.5, 20 mM EDTA, 1.4 M NaCl, 1% PEG 6000, 2% CTAB, 0.1% b-mercaptoethanol) heated at 74 °C in advance and incubated at 74 °C for 20 min inverting every 5 min. After incubation, when the sample was cooled down to room temperature, 20 ml of chloroform:isoamyalcohol (24:1) was added and mixed until homogenized and centrifuged at 3,000 rpm for 10 min. Then 20 ml of chloroform:isoamyalcohol (24:1) was added to the supernatant and mixed until homogenized. The sample was centrifuged at 3,000 rpm for 1 min and 20 ml of 2-propanol was added, mixed and incubated at 4 °C overnight. The sample was centrifuged at 3,500 rpm for 30 min and the supernatant was discarded. Next, 70% ethanol was added and centrifuged at 3,500 rpm for 10 min and the supernatant was discarded completely. The pellet was suspended with 1 ml of TE buffer on ice and 9 ml of Buffer G2 was added and mixed. Then, 18 µl of 100 mg ml^{-1} RNase A was added to the tube and incubated at 37 °C for 30 min. Next, 90 µl of proteinase K (Qiagen) was added to the sample and incubated for 50 °C for 1 h. After centrifugation at 10,000*g*, the supernatant was purified with Genomic-tip_100/G (Qiagen) following the manufacturer's protocol. Then, 0.7× volume of 2-propanol was added to the eluted DNA, inverted several times and centrifuged at 10,000*g* for 20 min. Next, 70% ethanol was added to the pellet and centrifuged at 10,000*g* for 20 min. The pellet was dissolved in 100 µl of TE buffer. Extracted DNA was quantified with Qubit double-stranded DNA High Sensitivity Assay kit (Thermo Fisher Scientific) and Nanodrop 2000 (Thermo Fisher Scientific).

Library preparation and analysis of PacBio sequencing

Extracted DNA was sheared with g-tube (Covaris). The SMRT library was prepared by SMRTbell express template prep kit (Pacific Bioscience) and the libraries were size selected (greater than 30 kb) using BluePippin system (Saga Science). The libraries were sequenced by PacBio Sequel (Pacific Bioscience) using Binding Kit v.3.0 and Sequencing Kit v.3.0 with the continuous long-read sequencing mode. One

SMRT cell (Sequel SMRT Cell 1 M v.3 LR) was used for each library and ran for 20 h. The SMRT sequencing data was generated at a coverage of 101×, N50 of 30,210 bp and a mean read length of 16,298 bp. The longest subreads were extracted from the sequencing data (682,486 subreads). The extracted subreads were mapped to 484 bp of the LTR sequence of *Tal1* (1,024 reads). The reads with less than 200 nucleotides (nt) of mapped region were removed from the analysis. The rest of the reads were mapped to Col-CEN reference genome[3] (ASM2311539v1 (GCA_023115395.1)) and 917 reads were mapped. Minimap2 (v.2.15-r905) was used for the mapping with the parameter '-c -x map-pb'. Among the 917 of mapped reads of *Tal1*(*ddm1*), the reads that had more than 3,560 bp (the length of 20 copies of CEN178) of the genomic sequence flanking *Tal1* were extracted. Many *Tal1* insertions are often detected in each PacBio read, but for the analyses here, we used only the best *Tal1* insertion match from each read. The number of *Tal1*-inserted site per 100 kbp of genomic sequence were counted.

Construction of CENH3 overexpression line

CENH3 overexpression line was generated as follows. For CENH3-OX-1, 2 and 4, CENH3 (At1g01370) coding region including intron was amplified from genomic DNA of wild-type Col-0. The amplified CENH3 fragment was introduced into XmaI/BamHI-digested pPLV01-pRPS5a vector that was generated by inserting pRPS5a promoter sequence in the *HpaI* site of pPLV01 vector[58]. For CENH3-OX-3, upstream region and coding region of CENH3 was amplified from genomic DNA of wild-type Col-0 and was introduced into XhoI/BamHI-digested pPLV01 vector. The primers used for the constructions are shown in Supplementary Table 4. The amplified CENH3 fragment and the digested vector were assembled using NEBuilder HiFi assembly Master Mix (NEB). The assembled product was introduced into the *Escherichia coli* DH5a strain by the heat shock method. The extracted plasmid was introduced into *Agrobacterium tumefaciens* GV3101::pMP90 by electroporation. The agrobacterium with transgene was introduced into *Arabidopsis* wild-type Col-0 by the floral dip method[59]. Transgenic T1 plants were selected in the Murashige and Skoog medium with 50 μg ml^{-1} of Basta. Plants with a homozygous transgene were selected in T2 plants. T2 or T3 plants were used for chromatin immunoprecipitation with sequencing (ChIP–seq).

Western blotting

Here, 0.5 g of 2-week-old seedlings from non-transgenic line (wild-type Col-0) or CENH3 overexpressing lines were ground into fine powder with liquid nitrogen, and nuclei were isolated by the method described previously[60]. Proteins were separated by 15% SDS–PAGE and then transferred to a polyvinyl difluoride (Cytiva) membrane using Trans-Blot SD Semi-Dry Cell (Bio-Rad). Primary antibodies against H3 (0.2 μg ml^{-1}; Abcam, ab1791), CENH3 C-terminal (0.2 μg ml^{-1}; affinity-purified rabbit polyclonal antibody against the peptide CRKDFELARRLGGKGRPW), HTR12 (CENH3 N-terminal) (0.25 μg ml^{-1}; affinity-purified rabbit polyclonal antibody against the peptide RTKHRVTRSQPRNQTDAC) and H4 (0.24 μg ml^{-1}; affinity-purified rabbit polyclonal antibody against the peptide CKRQGRTLYGFGG), and peroxidase-linked secondary antibody against rabbit IgG (1:10,000 dilution; Cytiva, NA934) were used for western blotting. Signals were developed using Western BLoT Quant Horse Radish Peroxidase Substrate (Takara) and detected using iBright Imaging System (Thermo Fisher Scientific).

Expression and purification of recombinant *Arabidopsis* H3 and CENH3

The DNA fragment encoding AtCENH3 was inserted into the pET-15b vector (Novagen), in which the tobacco etch virus protease recognition site was introduced instead of removal of the thrombin recognition site. The expression and purification of *A. thaliana* H3.1 and CENH3 proteins were performed as described previously[61]. Purified recombinant AtH3 and AtCENH3 proteins (50 ng each) were used for the validation of antibodies used in this study.

CENH3 ChIP–seq

Here, 0.4–0.5 g of 2-week-old whole seedlings were frozen with liquid nitrogen, ground into fine powder with motor and pestle and lysed with fixing buffer (PBS with 1% formaldehyde, 0.3% Triton X-100, 1 mM Pefabloc SC (Roche) and cOmplete EDTA-free Protease Inhibitor Cocktail (Roche)). The suspension was rotated at room temperature for 10 min for crosslinking. Then 0.2 M of glycine was added for quenching and rotated for 5 min at room temperature. The sample was centrifuged at 5,000*g*, 4 °C for 5 min, the pellet was washed once with PBS and it was resuspended with low-salt ChIP buffer without Triton X-100 (50 mM HEPES-KOH, 150 mM NaCl, 1 mM EDTA, 0.1% sodium deoxycholate, 0.1% SDS) to make the volume 900 μl. The sample was divided equally into three tubes, and sheared into 200–600 bp sizes using the Picoruptor sonication device (Diagenode) with 12 cycles of 30 s on/30 s off. The sonicated samples were centrifuged at 20,000*g* at 4 °C for 10 min, and Triton X-100 was added to the supernatant (final concentration: 1%). The sonicated chromatin was incubated with 0.5 μg of anti-HTR12 (CENH3 N-terminal) antibody[62] overnight at 4 °C, and then incubated with Dynabeads Protein G (Veritas) at 4 °C for 2 h. The incubated beads were washed once with 1 ml of low-salt ChIP buffer (50 mM HEPES-KOH, 150 mM NaCl, 1 mM EDTA, 1% Triton X-100, 0.1% sodium deoxycholate, 0.1% SDS), twice with 1 ml of high-salt ChIP buffer (50 mM HEPES-KOH, 500 mM NaCl, 1 mM EDTA, 1% Triton X-100, 0.1% sodium deoxycholate, 0.1% SDS), once with 1 ml of LiCl buffer (10 mM Tris-HCl, pH 7.8, 1 mM EDTA, 0.25 M LiCl, 1% IGEPAL CA-630, 1% sodium deoxycholate) and once with 1 ml of TE buffer (10 mM Tris-HCl, pH 7.8, 1 mM EDTA), while rotating for 10 min at 4 °C each time. DNA was eluted in 100 μl of elution buffer (10 mM Tris-HCl, pH 7.8, 0.3 M NaCl, 5 mM EDTA, 0.5% SDS), incubated overnight at 65 °C and then purified with the Monarch PCR & DNA Cleanup kit (New England Biolabs). The DNA was quantified with the Qubit dsDNA High Sensitivity Assay kit (Thermo Fisher Scientific), and 1–2 ng of DNA was used for preparing library with ThruPLEX DNA-seq kit (Clontech). The libraries were sequenced using HiSeq X Ten sequencer (Illumina) or Novaseq X plus sequencer at Macrogen Japan Corp.

ChIP–seq analysis

ChIP–seq data was processed as previously described[63] with some modifications. The fastq file of ChIP–seq data was quality filtered using Trimmomatic (v.0.39)[64] and mapped to Col-CEN_v1.2 reference genome. Mapping was conducted with Bowtie2 (v.2.4.4)[51] with no option. The mapped data was converted to BAM files using SAMtools (v.1.6)[65] and converted to BED files using BEDTools (v.2.26.0)[52]. The number of reads overlapped with 10 kb bin of chromosomes were counted using coverage function of BEDTools to make bedgraph files. Signals were plotted in units of reads per million mapped reads using ggplot2 (v.3.4.4)[53] package in R software (v.4.3.2)[56]. Reads that aligned to the chloroplast or the mitochondrial genome were not included in normalization. In Figs. 2c–f and 3d, a few (less than seven in each panel) dots are out of the ranges shown. The range of TR region around each centromere follow previous analyses[3]. The range of pericentromeric (PC) region surrounding each centromeric TR is defined as continuous 10 kb block with average mCHG > 0.25.

DNA methylation profiling by ONT

DNA methylation profiling of genomes including the centromeric TR regions has been performed as described previously[3]. Three weeks old seeding were ground in liquid nitrogen and the DNA was extracted using NucleoBond HMW DNA kit (MACHEREY-NAGEL) as per the manufacturer's instructions. A sequencing library was prepared using LSK-110 ligation kit, and sequenced using two MinION R9 flowcells. Methylation calling was performed as previously reported[66] with the modification that R9 reads were filtered for length and accuracy using Filtlong (v.0.2.0) (--min_mean_q 90, --min_length 5,000) and methylation prediction for the CG, CHG and CHH contexts were called using

DeepSignal-plant (v.1.6.1) using the model: model.dp2.CNN.arabnrice2-1_120m_R9.4plus_tem.bn13_sn16.both_bilstm.epoch6.ckpt.

Constructions of chimeric retrotransposons

To generate each construct of chimeric retrotransposons, DNA fragments were amplified by PCR using the plasmid *Tal1*_pRI909 (ref. 27) or *EVADE*_pRI909 as templates. To obtain *Evade*_pRI909 that contains a full length of *EVADE* (AT5TE20395, 5,329 bp), the 5′ half and 3′ half of AT5TE20395 were amplified by nested PCR from *A. thaliana* Col-0 genome using primers with the sites of restriction enzyme as shown in Supplementary Table 4. Second PCR products were digested with restriction enzymes: PstI and EcoRI for the 5′ half fragment, and EcoRI and BamHI for the 3′ half fragment. Both fragments and pRI909 binary vector (Takara) digested by PstI and BamHI were ligated with Mighty Mix (Takara). The plasmids and primers used in the construction of the chimeric retrotransposons are shown in Supplementary Table 4. PCR-amplified fragments and HpaI-linearized pPLV02 vector or pPLV03 (ref. 58) vector were separated by electrophoresis. The gel bands were extracted and purified by QIAquick Gel Extraction Kit (Qiagen) or Fastgene Gel/PCR Extraction Kit (Fastgene). Purified DNA fragments were assembled into a pPLV02 or pPLV03 vector using NEBuilder HiFi DNA assembly (New England Biolabs) and cloned in *E. coli*. Transgenic lines were generated by *Agrobacterium*-mediated gene transfer as described previously[27]. To confirm the activation of the introduced TE, the presence of extrachromosomal circular DNA of the TE in the transgenic plants was examined by PCR[67]. The primers and conditions used for the PCR are shown in Supplementary Table 4.

Analysis of nucleotide sequence bias around integration sites of *EVD* and *Tal1*

To examine local integration bias of *EVD* and *Tal1*, the region around integration site of each TE was extracted as follows. TE sequence in Read1 of TEd-seq reads (61 bp of 5′ terminals sequence for *EVD* or 41 bp of 5′ terminal sequence for *Tal1*) were trimmed with Cutadapt 4.4 (ref. 68) with the parameter '-gGCCCACTCTCTTGTAGTACATATCCAATACTAGGCCTTTCTTATTTGAGTCTTGATCAATA-m 30' for *Evade* and '-gATGTACGGATGGGTGCTTCACTCTTCGTTTCTTGATCAATA-m 30' for *Tal1*. The trimmed reads were mapped to the Col-CEN_v1.2 reference genome using Bowtie2 (v.2.5.1) with the parameter '--local --very-sensitive', and the mapped data was converted to BAM files using SAMtools (v.1.17). The central position of 5 bp target site duplication shown in Extended Data Fig. 9 was regarded as position zero. Next, 11 bp of integration site (−5 to +5 nucleotides from the centre of target site duplication) was extracted from Col-CEN_v1.2 using the 'getfasta' function of BEDTools (v.2.31.0). The number and the ratio of each nucleotide at each position in the 11 bp of integrated region were calculated.

Annotation of *Arabidopsis* LTR elements

TEs were identified for the NT1 and MN47 natural accessions of *A. lyrata* and for the Col-CEN reference genome of *A. thaliana* using the the Extensive De novo TE Annotator pipeline (v.2.0.1)[69] with parameters --anno 1 and --sensitive 1, and the Repbase[70] Arabidopsis-specific TE library (athrep.ref) as --curatedlib. Intact *Ty1*/*Copia* (110 in Col-CEN, 699 in NT1 and 800 in MN47) and *Ty3* (96, 830 and 1,029) LTR retrotransposons were further classified into lineages using TEsorter 1.3 (-db rexdb-plant -nolib)[71]. For all analysis, we removed elements that did not have consistent superfamily classification between Extensive De novo TE Annotator and TEsorter (for example, an element needed to be classified as *Ty3* by both pipelines). Following this approach, we retrieved 55, 393 and 295 *ALE* in Col-CEN, NT1 and MN47, respectively, and 49, 340 and 287 *ATHILA*.

Phylogenetic analysis and characterization of *ALE* and *ATHILA*

For the phylogenetic analysis, we further kept the subset of *ALE* (47, 368, 276) and *ATHILA* (11, 112, 71) that contained in correct order the hidden Markov models of all five genes (gag, protease, integrase, reverse transcriptase and RNaseH) according to TEsorter. For *ATHILA*, we also kept elements that contained only the gag and protease genes (35, 207, 205), because they represent a non-autonomous deletion derivative that is found in high numbers in *A. thaliana* and *A. lyrata*[5]. For *ALE*, we aligned the concatenated integrase and reverse transcriptase hidden Markov model domains retrieved from TEsorter for *ALE* with MAFFT (v.7.453, --globalpair --maxiterate 1,000)[72]. For *ATHILA*, we aligned the full-length DNA sequences with MAFFT (v.7.453, --retree 2 --maxiterate 50), so that elements that lacked the integrase, reverse transcriptase and RNaseH could be included in the tree. We used FastTree (v.2.1.11)[73] with default parameters to generate maximum-likelihood trees.

The age of LTR retrotransposons was estimated using the sequence divergence between the two LTRs of an intact element. A pairwise alignment was produced for each pair of LTR sequences using MUSCLE (v.3.8.1551)[74]. We used the recent dataset of *ATHILA* based on the annotation of 66 *A. thaliana* accessions[5]. To identify the R/K polymorphism in the *ALE4* branch, we looked for open reading frames with getorf from the EMBOSS:6.6.0.0 (ref. 75) using the internal region of every element. As in the phylogenetic analysis, we only surveyed elements that included all five genes. We focused on the longest open reading frame to examine and catalogue the R or K presence at the C-terminal end of the integrase gene with a custom R script. Downstream analyses were performed and plotted in R language and environment[56], using packages included in Tidyverse collection (v.2.0.0)[76], circlize (v.0.4.15)[77] and ggtree (v.3.10.0)[78].

Characterization of *ALE4*-like elements in other species

Sequences related to *EVD* and *Tal1* were retrieved from *Barbarea vulgaris* (GCA_963667165.1), *Eutrema japonicum* (GCA_030161315.1 and GCA_030161335.1)[79] and *Raphanus sativus* (GCF_000801105.2)[80]. The reverse transcriptase core domain region from *A. thaliana* COPIA20 was used to query the homology search by tBLASTn. Sequences with values less than 1×10^{-50} (for *B. vulgaris* and *R. sativus*) or 1×10^{-80} (for *E. japonicum*) were retrieved from genomic sequence assembly for analyses. Sequences including both 10 kb regions from the BLAST hit regions were obtained from genome assemblies to check presence of satellite sequences. The reverse transcription core domain regions were aligned for constructing phylogenetic trees. Aligned sequences were checked manually to delete sequences with more than 100 bp ambiguous or missing sites. Phylogenetic trees for reverse transcription regions were constructed by the neighbour-joining method with p-distances. *EVD*, AT1TE54585 (*COPIA93*) and AT2TE13385 (*COPIA20*) from *A. thaliana* and consensus sequences from clusters 1 to 4 of *copia93/20* sequences from *A. lyrata* with other *A. thaliana* COPIA families (*COPIA92*, *COPIA67*, *COPIA5*, *COPIA49*, *COPIA33*, *COPIA69*, *COPIA63*, *COPIA45* and *COPIA35*) were also included. All phylogenetic analyses were done by MEGA v.7.0 (ref. 81).

Reporting summary

Further information on research design is available in the Nature Portfolio Reporting Summary linked to this article.

Data availability

The TEd-seq data and ChIP–seq data have been deposited at National Center for Biotechnology Information Gene Expression Omnibus database with accession numbers GSE263224 and GSE263225, respectively. The accession number of the *Tal1* sequence is LC713258 ((DDBJ), (NCBI)). The PacBio data have been deposited with links to BioProject accession number PRJDB18115 in the DDBJ BioProject database. Uncropped images of western blot analyses are provided as Supplementary Figs. 3–5. Data files used for generating results in Figs. 1 and 4d and Extended Data Fig. 8 are available at Zenodo (https://doi.org/10.5281/zenodo.12627139)[82].

Code availability

Source code for the TEd-seq analysis is available at GitHub (https://github.com/LeanQ/TED_seq_Tsukahara_2024). Code used for generating results in Figs. 1 and 4d and Extended Data Fig. 8 are available at Zenodo (https://doi.org/10.5281/zenodo.12627139)[82].

50. Vendrell-Mir, P., Leduque, B. & Quadrana, L. Ultra-sensitive detection of transposon insertions across multiple families by transposable element display sequencing. Preprint at *bioRxiv* https://doi.org/10.1101/2024.08.21.608910 (2024).
51. Langmead, B. & Salzberg, S. L. Fast gapped-read alignment with Bowtie 2. *Nat. Methods* **9**, 357–359 (2012).
52. Quinlan, A. R. & Hall, I. M. BEDTools: a flexible suite of utilities for comparing genomic features. *Bioinformatics* **26**, 841–842 (2010).
53. Wickham, H. *Ggplot2: Elegant Graphics for Data Analysis* (Springer, 2016).
54. Wickham, H., Hester, J. & Bryan, J. readr: Read rectangular text data. R package version 2.1.5 (2024).
55. Wickham, H., François, R., Henry, L., Müller, K. & Vaughan, D. dplyr: A grammar of data manipulation. R package version 1.1.4 (2024).
56. R Core Team. *R: A Language and Environment for Statistical Computing* (R Foundation for Statistical Computing, 2023).
57. Murray, M. G. & Thompson, W. F. Rapid isolation of high molecular weight plant DNA. *Nucleic Acids Res.* **8**, 4321–4325 (1980).
58. De Rybel, B. et al. A versatile set of ligation-independent cloning vectors for functional studies in plants. *Plant Physiol.* **156**, 1292–1299 (2011).
59. Clough, S. J. & Bent, A. F. Floral dip: a simplified method for *Agrobacterium*-mediated transformation of *Arabidopsis thaliana*. *Plant J.* **16**, 735–743 (1998).
60. Lorković, Z. J. et al. Compartmentalization of DNA damage response between heterochromatin and euchromatin is mediated by distinct H2A histone variants. *Curr. Biol.* **27**, 1192–1199 (2017).
61. Osakabe, A. et al. Histone H2A variants confer specific properties to nucleosomes and impact on chromatin accessibility. *Nucleic Acids Res.* **46**, 7675–7685 (2018).
62. Talbert, P. B., Masuelli, R., Tyagi, A. P., Comai, L. & Henikoff, S. Centromeric localization and adaptive evolution of an *Arabidopsis* histone H3 variant. *Plant Cell* **14**, 1053–1066 (2002).
63. Inagaki, S., Takahashi, M., Takashima, K., Oya, S. & Kakutani, T. Chromatin-based mechanisms to coordinate convergent overlapping transcription. *Nat. Plants* **7**, 295–302 (2021).
64. Bolger, A. M., Lohse, M. & Usadel, B. Trimmomatic: a flexible trimmer for Illumina sequence data. *Bioinformatics* **30**, 2114–2120 (2014).
65. Li, H. et al. The Sequence Alignment/Map format and SAMtools. *Bioinformatics* **25**, 2078–2079 (2009).
66. Fernandes, J. B. et al. Structural variation and DNA methylation shape the centromere-proximal meiotic crossover landscape in *Arabidopsis*. *Genome Biol.* **25**, 30 (2024).
67. Reinders, J., Mirouze, M., Nicolet, J. & Paszkowski, J. Parent-of-origin control of transgenerational retrotransposon proliferation in *Arabidopsis*. *EMBO Rep.* **14**, 823–828 (2013).
68. Martin, M. Cutadapt removes adapter sequences from high-throughput sequencing reads. *EMBnet J.* **17**, 10 (2011).
69. Ou, S. et al. Benchmarking transposable element annotation methods for creation of a streamlined, comprehensive pipeline. *Genome Biol.* **20**, 275 (2019).
70. Bao, W., Kojima, K. K. & Kohany, O. Repbase Update, a database of repetitive elements in eukaryotic genomes. *Mob. DNA* **6**, 11 (2015).
71. Zhang, R.-G. et al. TEsorter: an accurate and fast method to classify LTR-retrotransposons in plant genomes. *Hortic. Res.* **9**, uhac017 (2022).
72. Katoh, K. & Standley, D. M. MAFFT multiple sequence alignment software version 7: improvements in performance and usability. *Mol. Biol. Evol.* **30**, 772–780 (2013).
73. Liu, K., Linder, C. R. & Warnow, T. RAxML and FastTree: comparing two methods for large-scale maximum likelihood phylogeny estimation. *PLoS ONE* **6**, e27731 (2011).
74. Edgar, R. C. MUSCLE: a multiple sequence alignment method with reduced time and space complexity. *BMC Bioinformatics* **5**, 113 (2004).
75. Rice, P., Longden, I. & Bleasby, A. EMBOSS: the European molecular biology open software suite. *Trends Genet.* **16**, 276–277 (2000).
76. Wickham, H. et al. Welcome to the tidyverse. *J. Open Source Softw.* **4**, 1686 (2019).
77. Gu, Z., Gu, L., Eils, R., Schlesner, M. & Brors, B. circlize implements and enhances circular visualization in R. *Bioinformatics* **30**, 2811–2812 (2014).
78. Yu, G., Smith, D. K., Zhu, H., Guan, Y. & Lam, T. T. GGTREE: an R package for visualization and annotation of phylogenetic trees with their covariates and other associated data. *Methods Ecol. Evol.* **8**, 28–36 (2017).
79. Tanaka, H. et al. Haplotype-resolved chromosomal-level assembly of wasabi (*Eutrema japonicum*) genome. *Sci. Data* **10**, 441 (2023).
80. Yu, H.-J., Baek, S., Lee, Y.-J., Cho, A. & Mun, J.-H. The radish genome database (RadishGD): an integrated information resource for radish genomics. *Database* **2019**, baz009 (2019).
81. Kumar, S., Stecher, G. & Tamura, K. MEGA7: Molecular Evolutionary Genetics Analysis version 7.0 for bigger datasets. *Mol. Biol. Evol.* **33**, 1870–1874 (2016).
82. Bousios, A. & Perez-Roman, E. BousiosLab/Centrophilic retrotransposons in *Arabidopsis*. *Zenodo* https://doi.org/10.5281/zenodo.12627139 (2024).

Acknowledgements We thank T. Sasaki for helpful advice and providing pPLV01-pRPS5a vector, A. Terui for technical assistance, and NASC/ABRC for distributing the seeds. The computations were partially performed on the NIG (National Institute of Genetics) supercomputer at NIG, Japan. This work was supported by grants from Human Frontier Science Program (HFSP) (RGP0025/2021) to I.H. and T.K., BBSRC (BB/V003984/1) to I.H., Japan Science and Technology Agency (JST) CREST (JPMJCR15O1) to T.K., PREST (JPMJPR20K3) to A.O., Japan Society for the Promotion of Science (JSPS) (22KJ0502 to S. Tsukahara, 22H04925 to A.T., 21K06284 to A.K., 21H04977 and 23H00365 to T.K.), Royal Society awards (UF160222, RF/ERE/221032, URF/R/221024, RGF/R1/180006, RGF/EA/201030 and RF/ERE/210069) to A.B. and Centre National de la Recherche Scientifique (IRP SYNERTE) to L.Q.

Author contributions A.B. and E.P.-R. designed and performed the analysis shown in Figs. 1 and 4d and Extended Data Figs. 1 and 8. For the other parts, S. Tsukahara, S.Y., B.L., A.N., M.N., A.O., A.T. and S.I. designed and performed the experiments and analysed the data. A.E. and S.O. analysed the data. H.I., S. Tominaga, J. and K.K. performed the experiments. Z.L., K.N. and F.B. provided the antibodies. A.K., L.Q., I.H. and T.K. conceived the project and analysed the data. S. Tsukahara and T.K. wrote the manuscript with incorporating opinions of the other authors.

Competing interests The authors declare no competing interests.

Additional information

Supplementary information The online version contains supplementary material available at https://doi.org/10.1038/s41586-024-08319-7.

Correspondence and requests for materials should be addressed to Sayuri Tsukahara, Alexandros Bousios or Tetsuji Kakutani.

Peer review information *Nature* thanks the anonymous reviewers for their contribution to the peer review of this work. Peer reviewer reports are available.

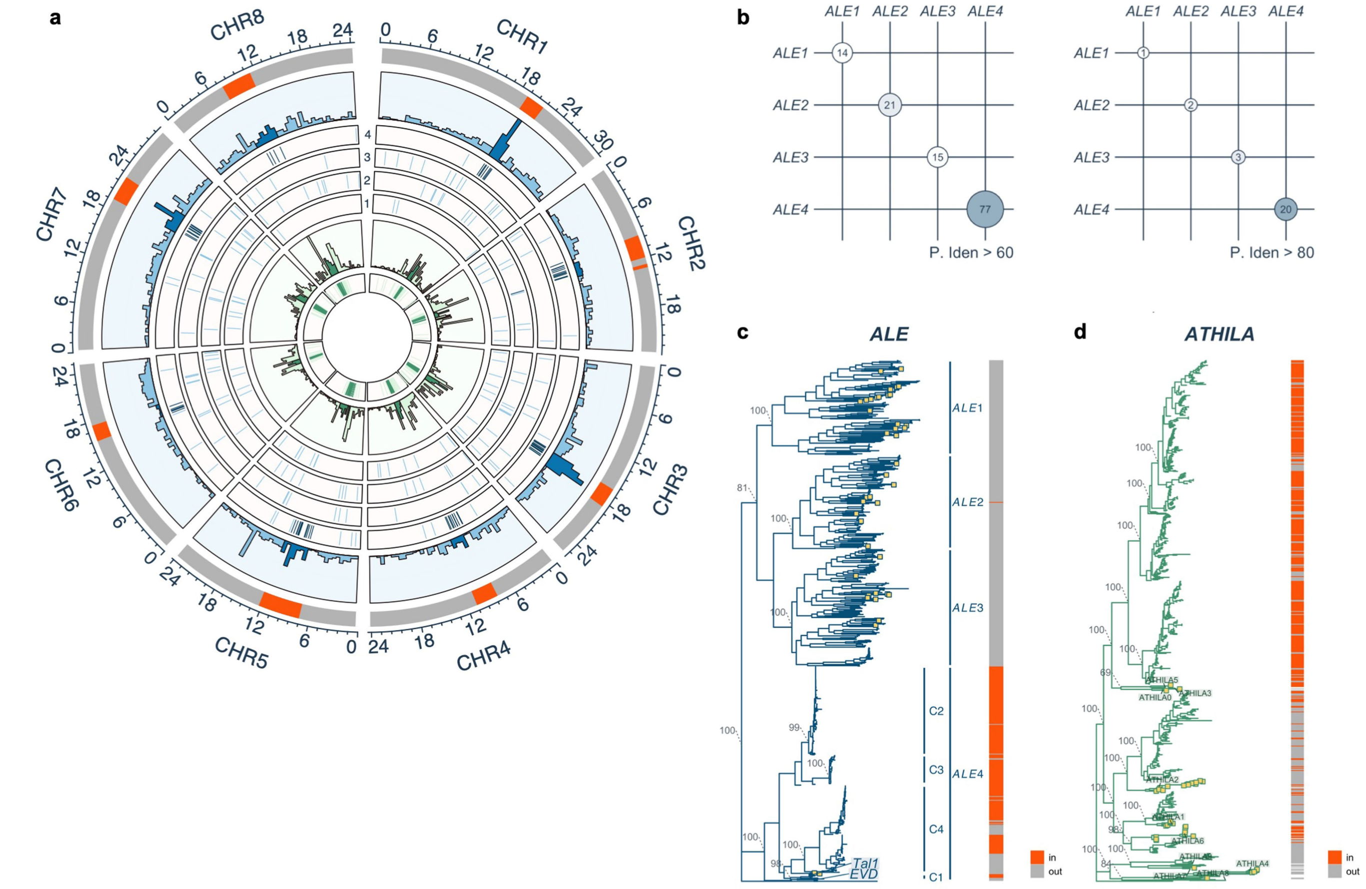

Extended Data Fig. 1 | *Arabidopsis lyrata* centromeres contain abundant LTR retrotransposons. **a**, Circos plot showing TE distribution along *A. lyrata* MN47 chromosomes. Orange blocks in outermost ribbon depict centromere-associated TR positions[5]. In all inner ribbons, *Ty1/Copia* and *Ty3* elements are shown with blue and green respectively, with darker shadings indicating insertions within the TRs. The second and seventh ribbon moving inwards show counts of intact *Ty1/Copia* and *Ty3* elements, computed separately for inside and outside of the TR regions using a bin width of ~600 kbp. All other ribbons show individual elements of the four main *ALE* branches (based on Fig. 1e) and of *ATHILA*[5]. **b**, Levels of pairwise sequence similarity between and within *ALE* branches with a 60% and 80% identity threshold. *ALE4* show high proportion of the sequence similarity within the group. **c**, *ALE* phylogenetic tree as in Fig. 1d. Additional adjacent strips (C1-4) show the centromeric Clusters 1-4 in previous publication[27] that correspond to *ALE4*. **d**, As the *ALE* tree but showing phylogeny of intact *ATHILA* based on their full-length sequence. The tree was rooted with the *Ty3* element (M34549.1) from *S. cerevisiae*. For both trees, bootstrap support of key nodes and known/consensus elements are indicated.

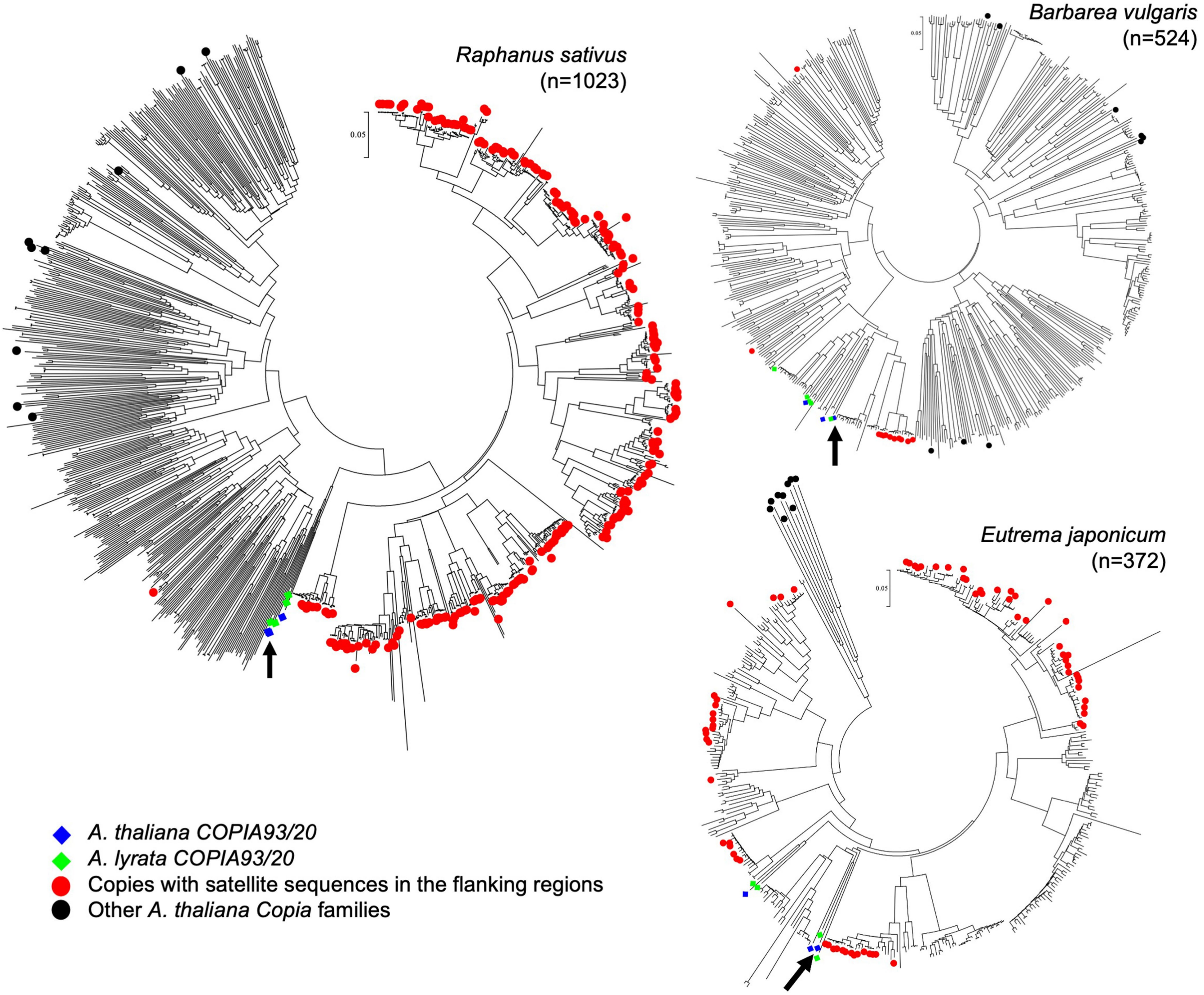

Extended Data Fig. 2 | Phylogenetic analyses of *ALE*-like sequences from three species related to *Arabidopsis*. The phylogenetic relationships of RT core domain sequences were represented by NJ trees. Number of sequences from each species was shown after species name in parenthesis. Red circles show copies flanking TR regions of each species. Also included are *Arabidopsis COPIA* sequences, such as consensus sequences of four *A. lyrata* centrophilic *ALE4* copies (green diamonds; C1-4[27]), related *A. thaliana* copies (blue diamonds), and a few other *A. thaliana COPIA* copies (black circles). An arrow indicates the position of *EVD*. Scale bars are shown beside the top of each tree. Centrophilic and centrophobic clusters are seen in each species. As is the case in *Arabidopsis ALE* copies, terminal branches in centrophilic clusters tend to be shorter than those in centrophobic clusters.

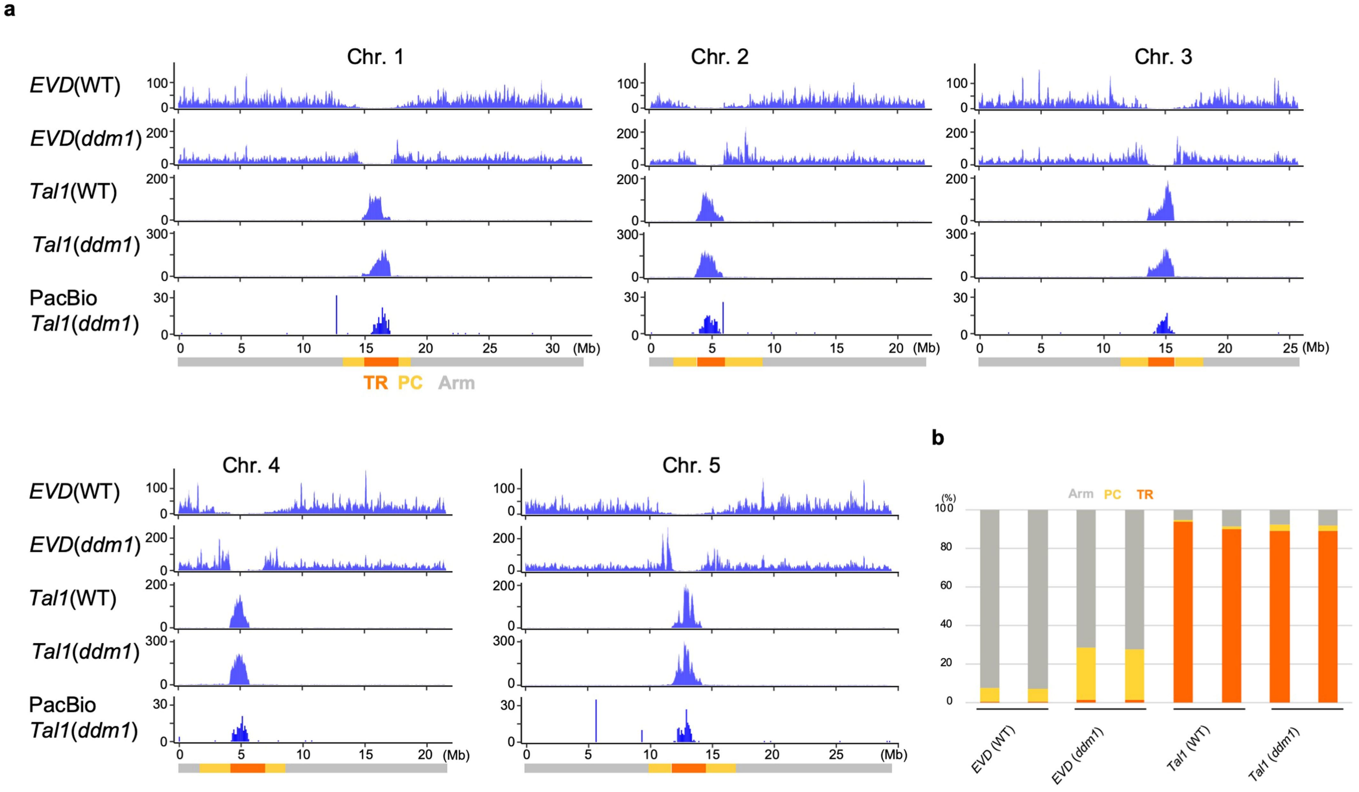

Extended Data Fig. 3 | De novo integration of *Tal1* in the central regions of the TR clusters, which are CENH3 occupied. a, Distributions of somatic neo-insertions of *EVD* and *Tal1* in the five chromosomes of *A. thaliana*. The format is as shown in Fig. 2b. **b**, As shown in Fig. 2g. Results of an additional independent line for each genotype are shown.

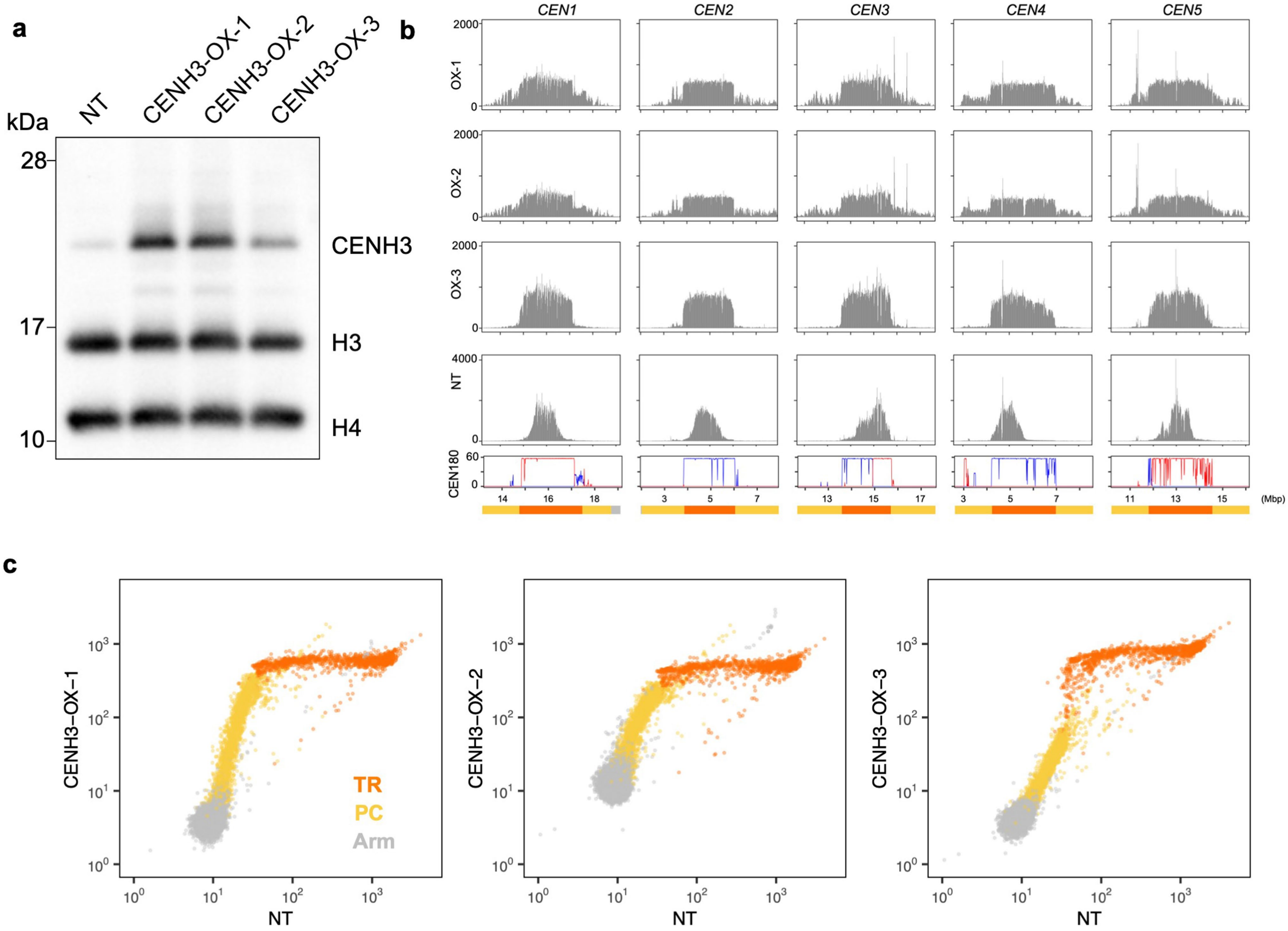

Extended Data Fig. 4 | CENH3 occupancy in CENH3 overexpression lines. **a**, Biological replicates of Western blot analysis in Fig. 3a. While Fig. 3a uses antibody recognizing CENH3 and H3 (CENH3 Cter), the results here use additional anti-H4 antibody. The line shown in Fig. 3 is CENH3-OX-1, and other independent transgenic lines, OX-2 and −3, were also examined here with the control non-transgenic (NT) line. OX-1 and OX-2 uses overexpression promoter, while OX-3 uses native promoter. Positions of molecular weight markers (28, 17, and 10 kDa) are shown in the left. Uncropped images of this panel and Fig. 3a are in Supplementary Figs. 4 and 3, respectively, with additional biological replicates. **b**, As in Fig. 3c, with additional CENH3-OX lines. **c**, As in Fig. 3d. OX-1 and OX-2 lines show saturation of CENH3 signals in the TR regions and increase of the signal in the PC regions. In OX-3, the increase was attenuated in the PC regions and periphery of the TR regions, while the effect is robust in the internal parts of the TR regions.

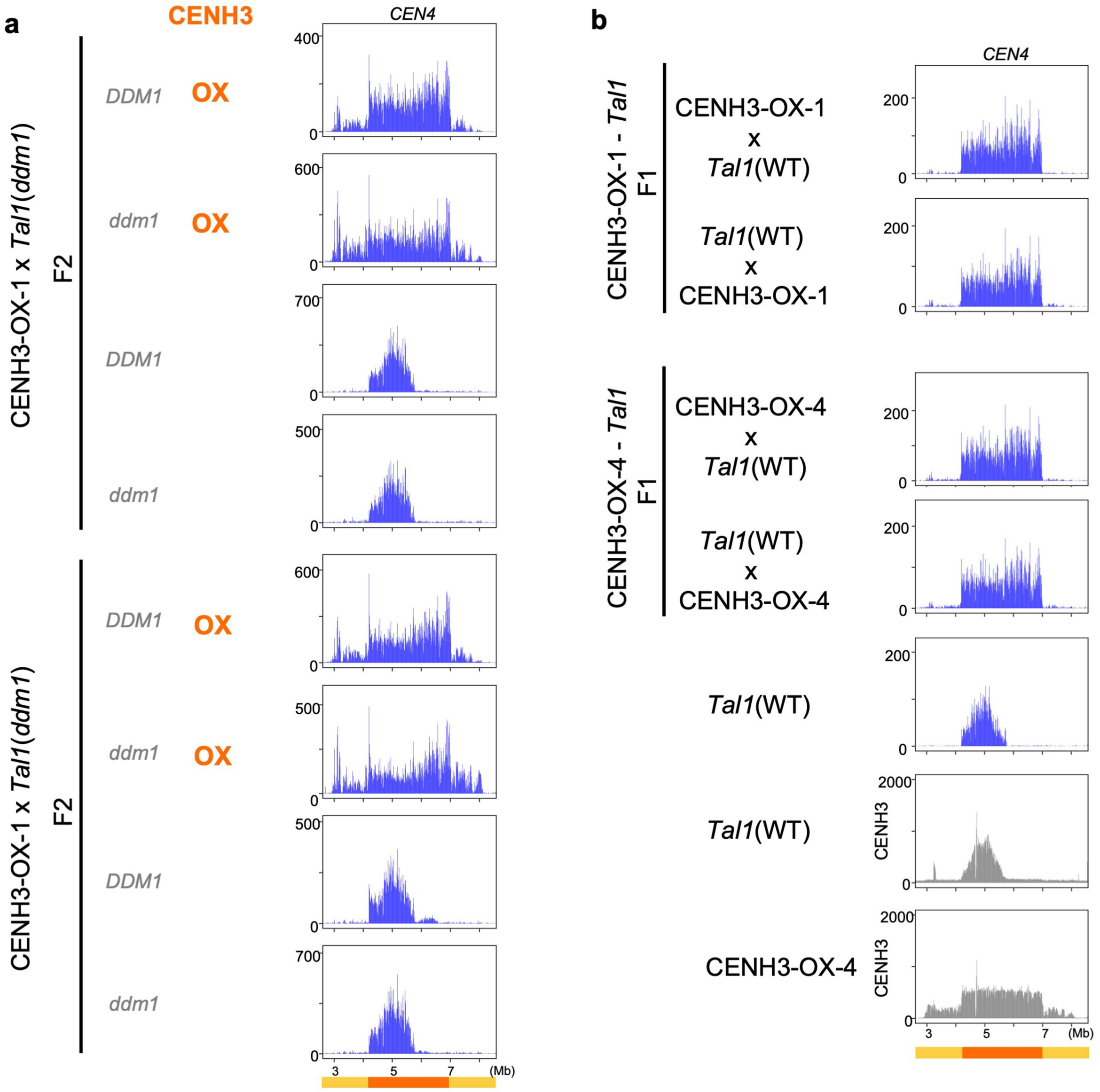

Extended Data Fig. 5 | *Tal1* integrations in F_2 and F_1 progenies from crosses between lines over-expressing CENH3 and *Tal1*. a, Distribution of *Tal1* integrations compared between sibling plants with and without the CENH3-OX transgene. Results of sibling plants in *DDM1* wild-type and the *ddm1* mutant backgrounds are shown for two F_2 families. **b**, *Tal1* neo-insertion in F_1 plants between different CENH3-OX lines and *Tal1* are examined for reciprocal crosses. The format as in Fig. 3f, with only *CEN4* region shown.

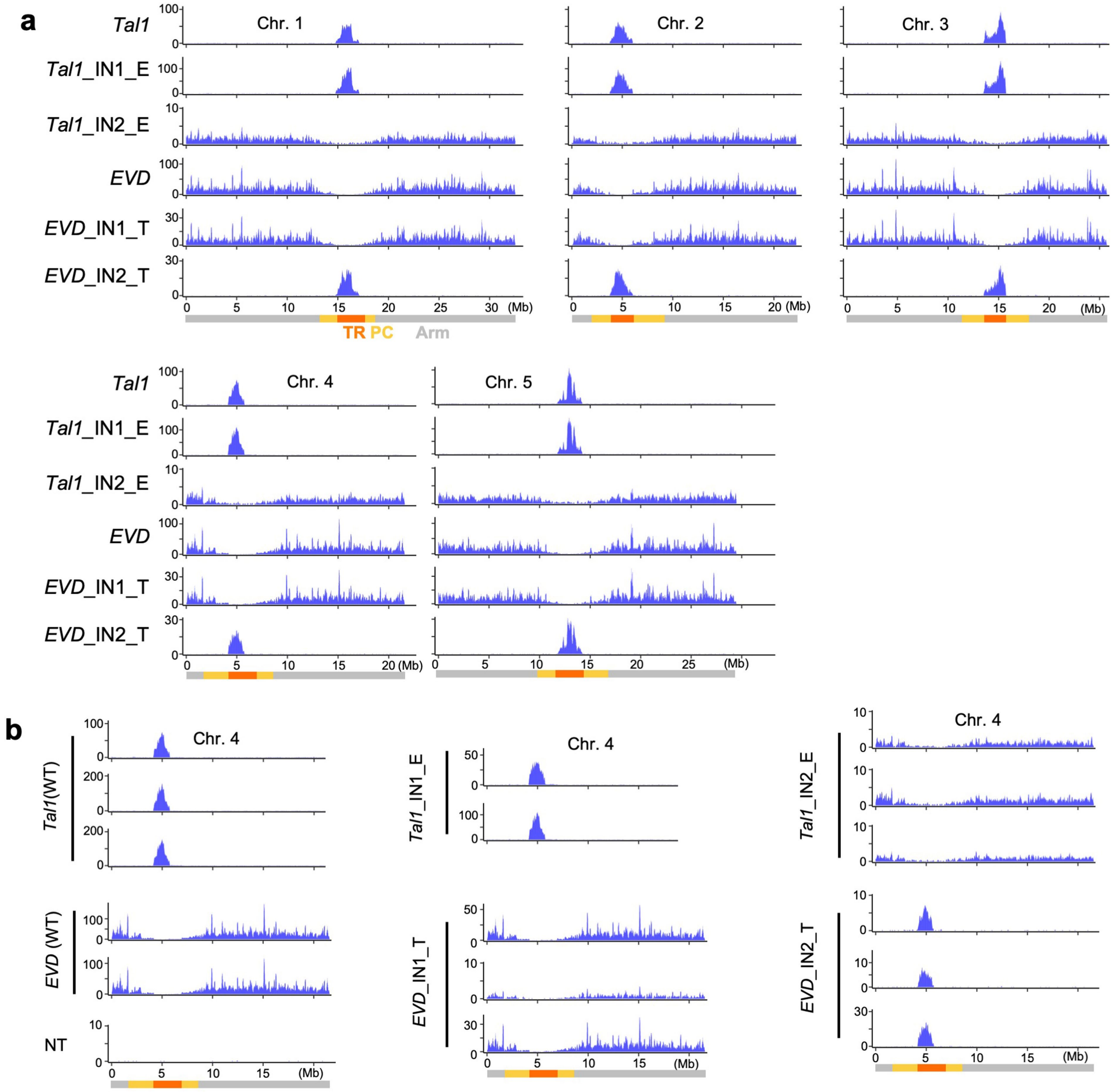

Extended Data Fig. 6 | Mapping of integrase regions that define the centrophilic versus centrophobic integrations of *Tal1* and *EVD*. The materials and format are as shown in Fig. 4a. **a**, Results of all five chromosomes. **b**, Results of multiple independent transgenic lines. Results of chromosome 4 are shown.

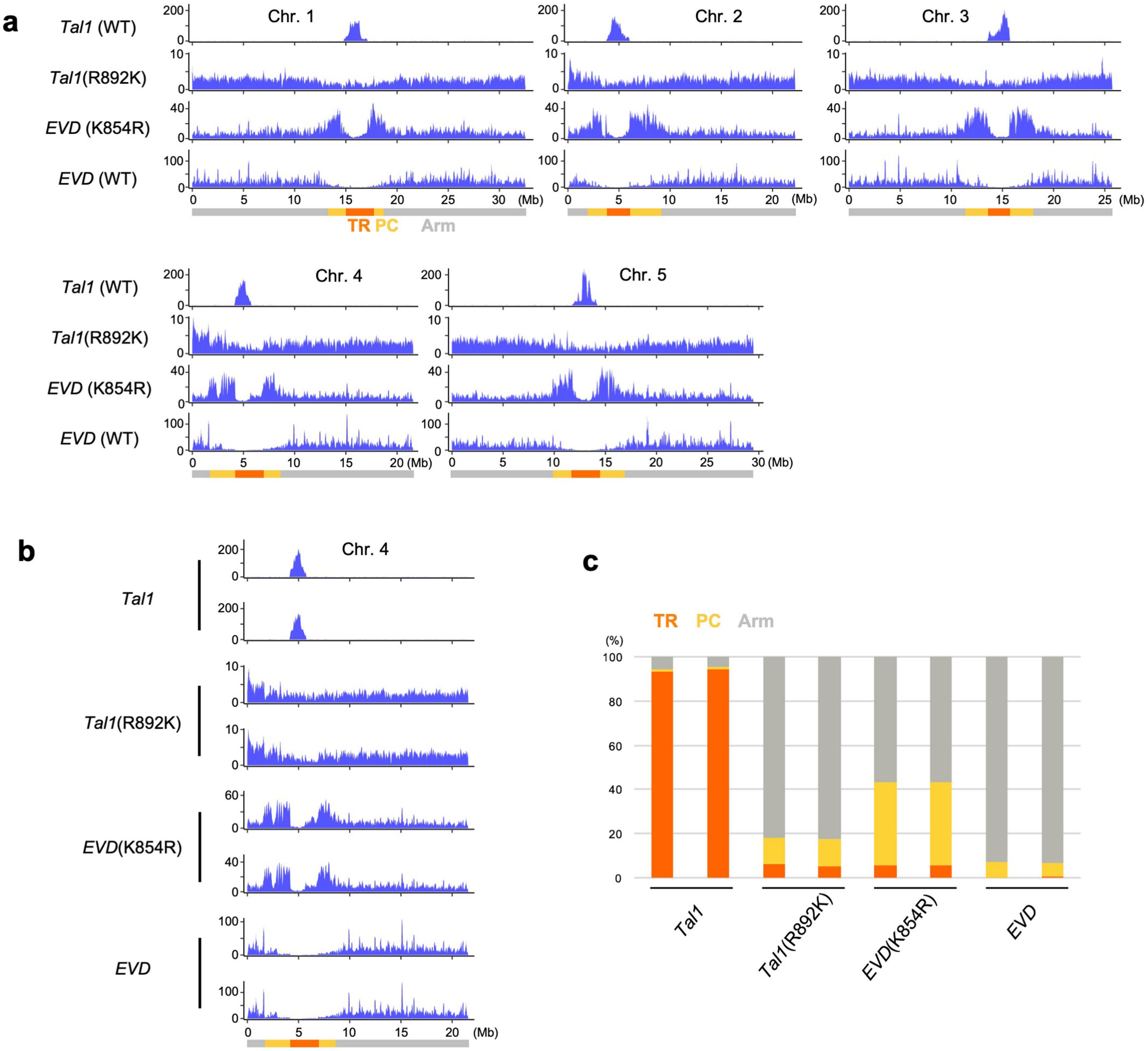

Extended Data Fig. 7 | R/K substitutions in *Tal1* or *EVD* integrase IN2 region changes integration specificities. The materials and format are as shown in Fig. 4b,c. **a**, As in Fig. 4b. Results of all five chromosomes are shown. **b, c**, As in Fig. 4b,c. Results of two biological replicates are shown.

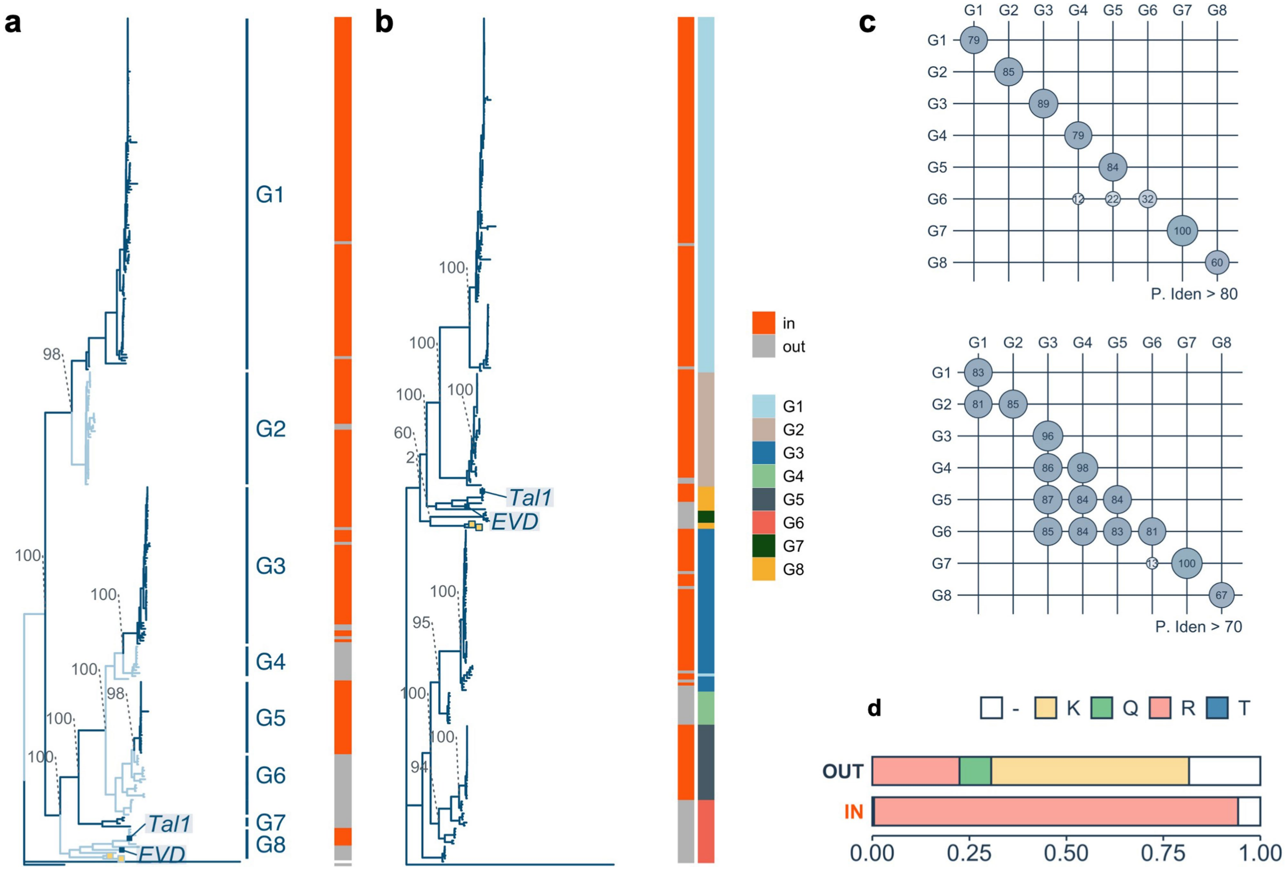

Extended Data Fig. 8 | *ALE4* phylogenetic trees. a, Same tree as in Fig. 4e based on the concatenated integrase (PF00665) and reverse transcriptase (PF07727) core domains. **b**, Tree generated by using the near complete length of the integrase gene. The longest open reading frame of every element the sequence between the first amino acid of the integrase core domain (PF00665) and immediately upstream of the first amino acid of the reverse transcriptase core domain (PF07727) is used. The G1-8 classification of the *ALE4* elements based on the 'a' tree are colour-coded in the 'b' tree to show that the branching pattern is consistent between the two trees (e.g. G1/G2 and G3-6 clustering). Bootstrap support of key nodes and the position of *Tal1* and *EVD* are shown. **c**, Levels of pairwise sequence similarity between and within G1-8 groups that exceed the 80% (top) and 70% (bottom) identity thresholds. G1-G2 and G3-6 share high levels of sequence similarity. **d**, Proportion of *ALE4* elements inside and outside the centromeric TRs that contain the R or K amino acid polymorphism. A small number contain Q. Blank parts reflect copies difficult to align.

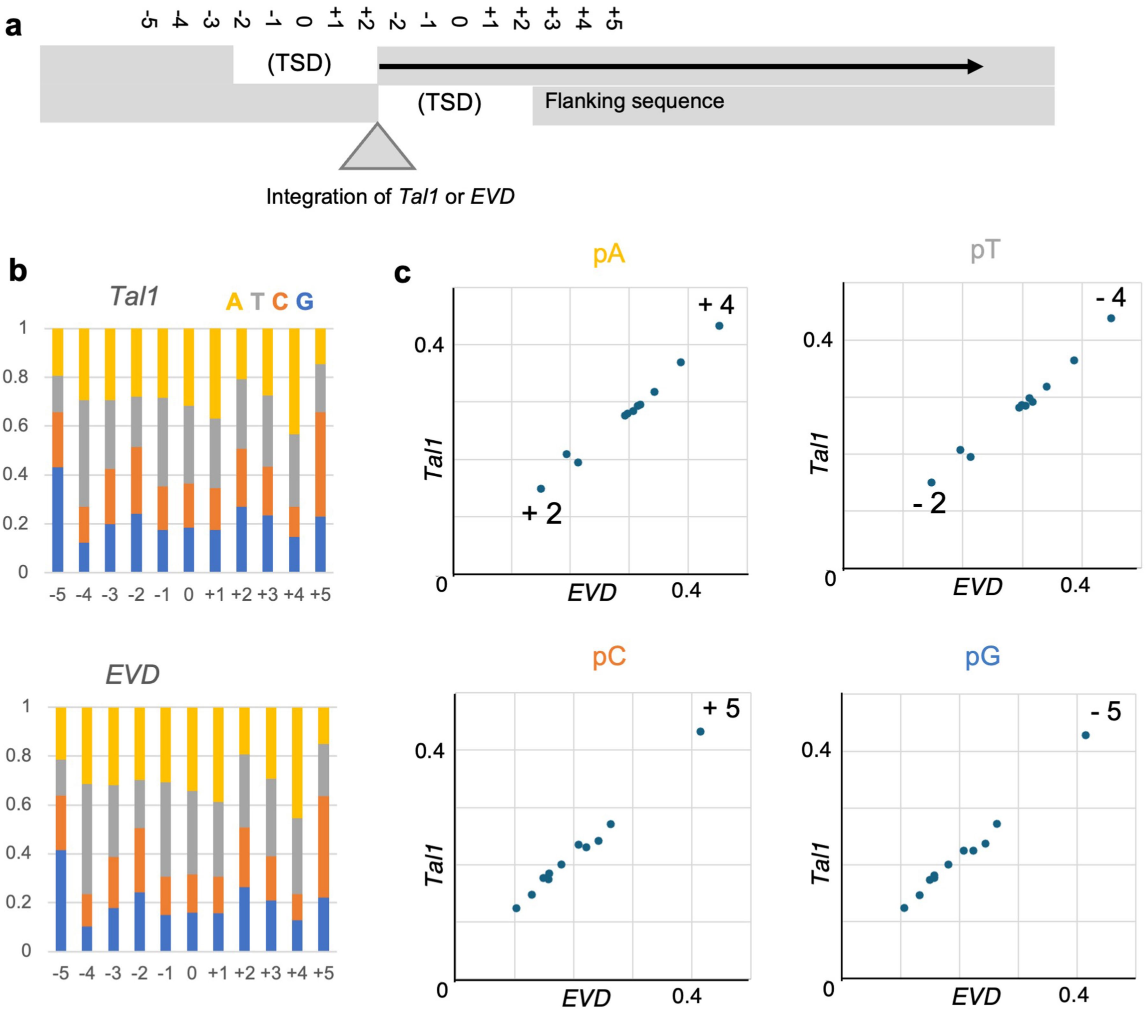

Extended Data Fig. 9 | *Tal1* and *EVD* show similar local integration bias. **a**, Schematic representation of the structure of retrotransposon integration sites. The integration site of the *copia* is shown by grey triangle; and the two strands of recipient genomic DNA are also shown by grey. As is the other *copia* elements, double strand break formation during transposon integration generates target site duplication (TSD) of five nucleotides. The central position of the TSD is counted as zero for estimating the integration site bias with keeping the symmetry. **b**, Nucleotide composition of −5 ~ +5 positions. The results are based on 108,545 of *EVD* integrations (bottom) and 23,228 of *Tal1* integrations outside the TR regions in the CENH3-OX line (top) are shown. **c**, The biases shown in the panel b are compared between *EVD* and *Tal1*. In the panels pA, pT, pC, or pG, each dot represents the proportion of each nucleotide at −5 ~ + 5 sites. The numbers are indicated for positions with strong bias, such as +4 and +2 of pA. It is also noted that the bias is detectable at symmetrical positions of pA-pT and pC-pG combinations.

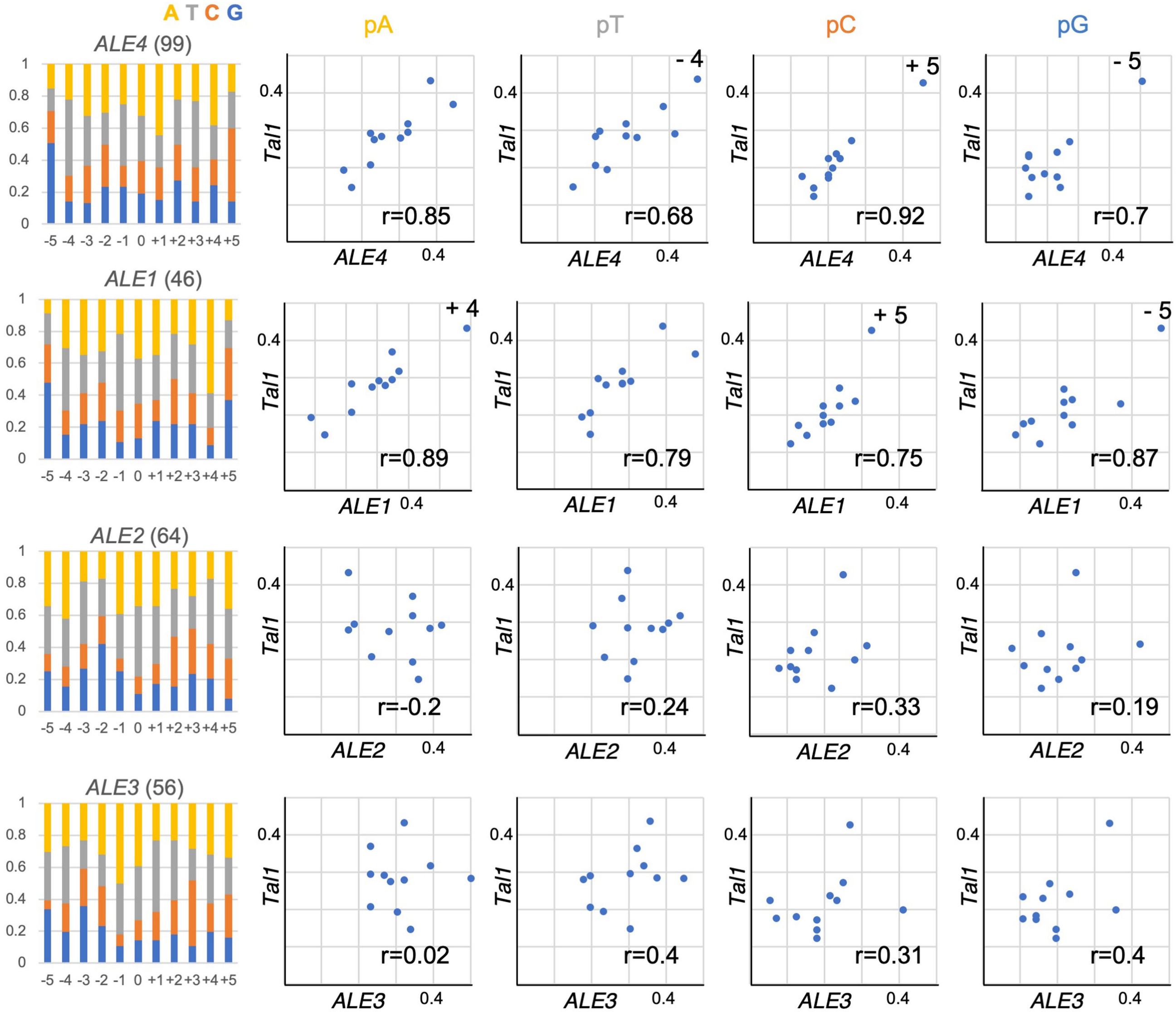

Extended Data Fig. 10 | Local integration bias in ALE1/2/3/4. As in Extended Data Fig. 9, integration bias of the *ALE* copies present in the MN47 genome were estimated and compared to that of *Tal1* neo-insertions. Number of each of *ALE* copies examined are shown in parenthesis. Pearson correlation coefficient (r) is shown for each graph. Integration bias of *Tal1* is conserved among *ALE4* (top). It is also conserved to *ALE1*, but they differ in *ALE2* and *ALE3*. The results suggest that local integration specificity evolves independent of the transitions of centrophilic/centrophobic properties.

nature portfolio

Corresponding author(s): Sayuri Tsukahara, Alexandros Bousios, Tetsuji Kakutani

Last updated by author(s): 8/25/2024

Reporting Summary

Nature Portfolio wishes to improve the reproducibility of the work that we publish. This form provides structure for consistency and transparency in reporting. For further information on Nature Portfolio policies, see our Editorial Policies and the Editorial Policy Checklist.

Statistics

For all statistical analyses, confirm that the following items are present in the figure legend, table legend, main text, or Methods section.

n/a	Confirmed	
□	☒	The exact sample size (*n*) for each experimental group/condition, given as a discrete number and unit of measurement
□	☒	A statement on whether measurements were taken from distinct samples or whether the same sample was measured repeatedly
☒	□	The statistical test(s) used AND whether they are one- or two-sided *Only common tests should be described solely by name; describe more complex techniques in the Methods section.*
☒	□	A description of all covariates tested
☒	□	A description of any assumptions or corrections, such as tests of normality and adjustment for multiple comparisons
□	☒	A full description of the statistical parameters including central tendency (e.g. means) or other basic estimates (e.g. regression coefficient) AND variation (e.g. standard deviation) or associated estimates of uncertainty (e.g. confidence intervals)
☒	□	For null hypothesis testing, the test statistic (e.g. *F*, *t*, *r*) with confidence intervals, effect sizes, degrees of freedom and *P* value noted *Give P values as exact values whenever suitable.*
☒	□	For Bayesian analysis, information on the choice of priors and Markov chain Monte Carlo settings
☒	□	For hierarchical and complex designs, identification of the appropriate level for tests and full reporting of outcomes
☒	□	Estimates of effect sizes (e.g. Cohen's *d*, Pearson's *r*), indicating how they were calculated

Our web collection on statistics for biologists contains articles on many of the points above.

Software and code

Policy information about availability of computer code

Data collection	Trimmomatic 0.39, Bowtie2 v.2.4.4 (for ChIP-seq), v.2.5.3 (for TED-seq), and v.2.5.1 (for analysis of nucleotide bias), Picard 2.27.5, Samtools 1.6 (for ChIP-seq), 1.9 (for TED-seq) and 1.7 (for analysis of nucleotide bias), Bedtools 2.26.0 (for ChIP-seq), 2.31.1 (for TED-seq), and 2.31.0 (for analysis of nucleotide bias) Cutadapt 4.4, Extensive De novo TE Annotator (EDTA) pipeline v2.0.1, TEsorter 1.3, MAFFT v7.453, FastTree v.2.1.11, MUSCLE v3.8.1551, EMBOSS v.6.6.0.0, MEGA ver 7.0, Filtlong Version 0.2.0, DeepSignal-plant v1.6.1, Minimap2 v2.15-r905, R software v.4.3.2, ggplot2 v.3.4.4, dplyr v1.1.4, readr v.2.1.5. Source code for the TEd-seq analysis (https://github.com/LeanQ/TED_seq_Tsukahara_2024). Data files and code used for generating results in Figure 1, 4d and Extended Data Figure 8 (https://zenodo.org/records/12627140).
Data analysis	Trimmomatic 0.39, Bowtie2 v.2.4.4 (for ChIP-seq), v.2.5.3 (for TED-seq), and v.2.5.1 (for analysis of nucleotide bias), Picard 2.27.5, Samtools 1.6 (for ChIP-seq), 1.9 (for TED-seq) and 1.7 (for analysis of nucleotide bias), Bedtools 2.26.0 (for ChIP-seq), 2.31.1 (for TED-seq), and 2.31.0 (for analysis of nucleotide bias) Cutadapt 4.4, Extensive De novo TE Annotator (EDTA) pipeline v2.0.1, TEsorter 1.3, MAFFT v7.453, FastTree v.2.1.11, MUSCLE v3.8.1551, EMBOSS v.6.6.0.0, MEGA ver 7.0, Filtlong Version 0.2.0, DeepSignal-plant v1.6.1, Minimap2 v2.15-r905, R software v.4.3.2, ggplot2 v.3.4.4, dplyr v1.1.4, readr v.2.1.5. Source code for the TEd-seq analysis (https://github.com/LeanQ/TED_seq_Tsukahara_2024). Data files and code used for generating results in Figure 1, 4d and Extended Data Figure 8 (https://zenodo.org/records/12627140).

For manuscripts utilizing custom algorithms or software that are central to the research but not yet described in published literature, software must be made available to editors and reviewers. We strongly encourage code deposition in a community repository (e.g. GitHub). See the Nature Portfolio guidelines for submitting code & software for further information.

Data

Policy information about availability of data

All manuscripts must include a data availability statement. This statement should provide the following information, where applicable:

- Accession codes, unique identifiers, or web links for publicly available datasets
- A description of any restrictions on data availability
- For clinical datasets or third party data, please ensure that the statement adheres to our policy

The TED-seq data and ChIP-seq data has been deposited at NCBI Gene Expression Omnibus (GEO) database with accession numbers GSE263224 and GSE263225, respectively.
Col-CEN reference genome is available at (https://github.com/schatzlab/Col-CEN).

Research involving human participants, their data, or biological material

Policy information about studies with human participants or human data. See also policy information about sex, gender (identity/presentation), and sexual orientation and race, ethnicity and racism.

Reporting on sex and gender	not applicable.
Reporting on race, ethnicity, or other socially relevant groupings	not applicable.
Population characteristics	not applicable.
Recruitment	not applicable.
Ethics oversight	not applicable.

Note that full information on the approval of the study protocol must also be provided in the manuscript.

Field-specific reporting

Please select the one below that is the best fit for your research. If you are not sure, read the appropriate sections before making your selection.

☒ Life sciences □ Behavioural & social sciences □ Ecological, evolutionary & environmental sciences

For a reference copy of the document with all sections, see nature.com/documents/nr-reporting-summary-flat.pdf

Life sciences study design

All studies must disclose on these points even when the disclosure is negative.

Sample size	Sample size calculation was not performed. Each sample contains pool of ≥5 plants, and multiple TED-seq and ChIP-seq gave reproducible results.
Data exclusions	As described in Methods part, the TED-seq data mapped within 1-30 kbp of chromosome 2 was excluded for the analysis because these were found in all samples, including wild-type controls, and therefore do not correspond to bona fide de novo insertions.
Replication	TED-seq and ChIP-seq have been performed with at least two biological replicates with essentially the same results.
Randomization	The plant materials were grown on agar plates under controlled conditions and they show similar morphological phenotypes, from which the samples were randomly chosen.
Blinding	Blinding was not applicable. For processing of sequencing libraries and all other computational data analyses, the same parameters were applied, during which no manual intervention occurs.

Reporting for specific materials, systems and methods

We require information from authors about some types of materials, experimental systems and methods used in many studies. Here, indicate whether each material, system or method listed is relevant to your study. If you are not sure if a list item applies to your research, read the appropriate section before selecting a response.

Materials & experimental systems

n/a	Involved in the study
□	☒ Antibodies
☒	□ Eukaryotic cell lines
☒	□ Palaeontology and archaeology
☒	□ Animals and other organisms
☒	□ Clinical data
☒	□ Dual use research of concern
□	☒ Plants

Methods

n/a	Involved in the study
□	☒ ChIP-seq
☒	□ Flow cytometry
☒	□ MRI-based neuroimaging

Antibodies

Antibodies used	For ChIP-seq, Anti-HTR12(CENH3 N-terminal) antibody (affinity-purified rabbit polyclonal antibody against the peptide RTKHRVTRSQPRNQTDAC) was used. Anti-HTR12(CENH3 N-terminal) antibody was previously used in Talbert et al., Plant Cell. 2002. For Western blotting, primary antibodies CENH3 C-terminal (0.2 µg/ml; affinity-purified rabbit polyclonal antibody against the peptide CRKDFELARRLGGKGRPW), H4 (0.24 µg/ml; affinity-purified rabbit polyclonal antibody against the peptide CKRQGRTLYGFGG), and peroxidase-linked secondary antibody against rabbit IgG (1:10.000 dilution; Cytiva, NA934) were used.
Validation	Western blotting was performed using recombinant AtH3 and AtCENH3 (50 ng) proteins to validate Anti-H3 antibody (0.2 µg/ml; Abcam, ab1791), Anti-HTR12(CENH3 N-terminal) antibody (0.25 µg/ml; affinity-purified rabbit polyclonal antibody against the peptide RTKHRVTRSQPRNQTDAC), and Anti-CENH3 C-terminal antibody (Supplementary Figure 1). Uncropped images of Western blotting results are in Supplementary Source Fig. 3.

Plants

Seed stocks	The Arabidopsis thaliana Columbia-0 (Col-0) accession of wild type and ddm1-1 mutant (Vongs et al., 1993 Science) were used.
Novel plant genotypes	CENH3 over-expression lines were generated by transforming the construct with CENH3 (At1g01370) coding region driven by RPS5a promoter or native promoter with binary vector pPLV01 into WT Col-0.
Authentication	Multiple CENH3 over-expression lines were used for each experiment. The results described were similar among the different lines.

ChIP-seq

Data deposition

☒ Confirm that both raw and final processed data have been deposited in a public database such as GEO.

☒ Confirm that you have deposited or provided access to graph files (e.g. BED files) for the called peaks.

Data access links *May remain private before publication.*	https://www.ncbi.nlm.nih.gov/geo/query/acc.cgi?acc=GSE263225
Files in database submission	CENH3-3_1.fastq.gz (WT Col-0) CENH3-3_2.fastq.gz (WT Col-0) CENH3-4_1.fastq.gz (CENH3-OX-1) CENH3-4_2.fastq.gz (CENH3-OX-1) CENH3-5_1.fastq.gz (CENH3-OX-2) CENH3-5_2.fastq.gz (CENH3-OX-2) CENH3-1_1.fastq.gz (CENH3-OX-3) CENH3-1_2.fastq.gz (CENH3-OX-3) CENH3-6_1.fastq.gz (CENH3-OX-4) CENH3-6_2.fastq.gz (CENH3-OX-4) Cenh3_23-204_1.fastq.gz (WT Col-0) Cenh3_23-204_2.fastq.gz (WT Col-0) Cenh3_23-206_1.fastq.gz (ddm1) Cenh3_23-206_2.fastq.gz (ddm1) Cenh3_23-207_1.fastq.gz (Tal1(WT)) Cenh3_23-207_2.fastq.gz (Tal1(WT)) Cenh3_23-208_1.fastq.gz (Tal1(ddm1)_1) Cenh3_23-208_2.fastq.gz (Tal1(ddm1)_1) Cenh3_23-194_1.fastq.gz (Tal1(ddm1)_2)

Cenh3_23-194_2.fastq.gz (Tal1(ddm1)_2)
Cenh3_23-195_1.fastq.gz (Tal1(ddm1)_3)
Cenh3_23-195_2.fastq.gz (Tal1(ddm1)_3)
CENH3-3_10kb_coverage.bedgraph
CENH3-4_10kb_coverage.bedgraph
CENH3-5_10kb_coverage.bedgraph
CENH3-1_10kb_coverage.bedgraph
CENH3-6_10kb_coverage.bedgraph
Cenh3_23-204_240329_10kb_coverage.bedgraph
Cenh3_23-206_240329_10kb_coverage.bedgraph
Cenh3_23-207_240329_10kb_coverage.bedgraph
Cenh3_23-208_240329_10kb_coverage.bedgraph
Cenh3_23-194_240329_10kb_coverage.bedgraph
Cenh3_23-195_240329_10kb_coverage.bedgraph

Genome browser session
(e.g. UCSC)

not applicable

Methodology

Replicates

4 lines of CENH3 OX lines and 4 lines of Tal1 transgenic lines were examined. 1 line of WT was analyzed in each ChIP-seq experiments.

Sequencing depth

The total number of reads and mapped reads are as follows. All reads were 151 bp of paired-end reads.
(WT Col-0) 56,266,808 reads, 29,181,568 reads,
(CENH3-OX-1) 56,808,062 reads, 33,033,093 reads,
(CENH3-OX-2) 60,418,556 reads, 36,201,138 reads,
(CENH3-OX-3) 46,951,246 reads, 21,799,866 reads,
(CENH3-OX-4) 56,923,758 reads, 33,051,380 reads,
(WT Col-0) 26,218,596 reads, 6,850,227 reads,
(ddm1) 28,125,766 reads, 5,480,001 reads,
(Tal1(WT)) 26,317,226 reads, 4,184,822 reads,
(Tal1(ddm1)_1) 26,868,658 reads, 4,753,096 reads,
(Tal1(ddm1)_2) 15,793,706 reads, 8,556,374 reads,
(Tal1(ddm1)_3) 23,631,674 reads, 7,484,412 reads,

Antibodies

Anti-HTR12(CENH3 Nter) antibody was used for ChIP-seq. It was validated as shown in Supplementary Figure 1.

Peak calling parameters

not applicable.

Data quality

Wild type non-transgenic control shows essentially the same pattern as that in previous publications (Naish et al 2021 Science; Wlodzimierz et al Nature 2023).

Software

The fastq file of ChIP-seq data was quality filtered with Trimmomatic (0.39) and mapped to Col-CEN_v1.2 reference genome. Mapping was conducted with Bowtie2 (v.2.4.4) with no option. The mapped data was converted to BAM files using SAMtools (v.1.6) and converted to BED files using BEDTools (v.2.26.0). The number of reads overlapped with 10 kb bin of chromosomes were counted using coverage function of BEDTools to make bedgraph files. Signals were plotted in units of reads per million mapped reads (RPM) using ggplot2 package in R software (v.4.3.2). Reads that aligned to the chloroplast or the mitochondrial genome were not included in normalization.